IEEE Access
Multidisciplinary | Rapid Review | Open Access Journal

Received January 2, 2018, accepted February 22, 2018, date of publication March 8, 2018, date of current version March 28, 2018.

Digital Object Identifier 10.1109/ACCESS.2018.2813313

A Unified Array Geometry Composed of Multiple Identical Subarrays With Hole-Free Difference Coarrays for Underdetermined DOA Estimation

MINGLEI YANG[1], (Member, IEEE), ALEXANDER M. HAIMOVICH[2], (Fellow, IEEE), XIN YUAN[3], (Senior Member, IEEE), LEI SUN[1], AND BAIXIAO CHEN[1]

[1]National Laboratory of Radar Signal Processing, Xidian University, Xi'an 710071, China
[2]Department of Electrical and Computer Engineering, New Jersey Institute of Technology, Newark, NJ 07102, USA
[3]Bell Labs, Murray Hill, NJ 07974, USA

Corresponding author: Minglei Yang (mlyang@xidian.edu.cn)

This work was supported in part by the National Natural Science Foundation of China under Grant 61571344, in part by the Fund for Foreign Scholars in University Research and Teaching Programs (the 111 Project) under Grant B18039, and in part by the China Scholarship Council.

ABSTRACT In this paper, we propose a unified array geometry, dubbed generalized nested subarray (GNSA), for the underdetermined direction-of-arrival estimation. The GNSA is composed of multiple, identical subarrays, which can be a minimum redundancy array (MRA), a (super) nested array, a uniform linear array (ULA), or any other linear arrays with hole-free difference coarrays (DCAs). By properly design the spacings between subarrays, the resulting DCA of the GNSA can also be a hole-free (filled) ULA. When the subarray is an MRA and meanwhile its sensors' positions also follow an MRA configuration, a nested MRA (NMRA) is constructed. This NMRA can provide up to $\mathcal{O}(M^2N^2)$ degrees of freedom (DOFs) using only MN physical sensors. In order to fully utilize the increased DOF, we develop a new DOA estimation algorithm, which consists of a dimensional reduction matrix to exploit the data of all virtual elements, a Toeplitz matrix to decorrelate the equivalent coherent sources, and a root-MUSIC method to mitigate the computational workload. This new algorithm can achieve better DOA estimation performance than traditional spatial smoothing MUSIC algorithm with lower computational complexity. Numerical simulation results demonstrate the superiorities of the proposed array geometry in resolving more sources than sensors, DOA estimation performance, and the angular resolution.

INDEX TERMS Coprime array, difference coarray, direction-of-arrival (DOA) estimation, minimum redundancy array, nested array, sensor arrays.

I. INTRODUCTION

Direction-of-arrival (DOA) estimation is an important topic in various applications, such as radar and sonar. It is well known that the maximum number of sources that can be resolved by a K-element uniform linear array (ULA) using traditional DOA estimation methods, such as MUSIC [1] and ESPRIT [2], is $K-1$. The underdetermined DOA estimation problem, *i.e.*, resolving more sources than sensors, has received considerable interest in recent years [3]–[6]. An effective approach to solve this problem is to increase the number of degree of freedom (DOF) by designing an equivalent virtual array (see, *e.g.*, [7]). The number of DOF is an important array design criteria because more DOFs mean more sources can be resolved by the array system. In principle, the virtual array is constructed by vectorizing the covariance matrix of the received data collected from a properly designed non-uniform linear array [7]–[11].

A. NON-UNIFORM LINEAR ARRAY DESIGN FOR DOA ESTIMATION

Various non-uniform linear array design methodologies have been reported in the literature, for example, the minimum redundancy array (MRA) [8], the nested array [7], and the coprime array [9], [10], *etc*. An MRA is a linear array designed to minimize the number of array elements by reducing the redundancy of the element spacing. The virtual array derived from an MRA is a hole-free ULA with the largest possible aperture for a given number (K) of physical sensors.

Unfortunately, no closed-form expressions for the sensor positions and for the number of achievable DOF as a function of K have reported in literature. Other relatively ad-hoc approaches exist, for example, design of MRAs for $K \leqslant 17$ sensors has been found by exhaustive search routines [9], [12]. Ishiguro [13] discussed a method of using a combination of two MRAs to find an MRA for a large number of antennas. However, only a constructing method with several combinations of the two MRAs is given. Therefore, a systematic mathematical tractable design approach for larger MRAs is lacking.

Recently, a new nested array (NA) design approach has been proposed [7]. Nested linear arrays are nonuniform arrays constructed by concatenating two or more ULAs where each of the subarray has a different inter-element spacing. One subarray has denser unit inter-element spacing than the other one. By using the second order statistics of the received sensor data, it is possible to achieve $\mathcal{O}(K^2)$ DOFs from K physical sensors. Moreover, there is a closed-form expression for sensor positions and computing DOFs [7], [14]. However, as reported in [9]–[11], a limitation of the NA approach is that the sensors in the first subarray of the nested array are usually closely located in space, which would lead to mutual coupling problems between adjacent sensors.

Most recently, a coprime array (CA) [9], [10], [15] consists of two uniform linear subarrays with M and N elements has been proposed, where M, N are coprime integers. The coprime array is capable of providing a higher number of DOF than the number of physical sensors, and it has the advantage of reducing mutual coupling between sensors by increasing the inter-element spacing. One can also create a virtual array from a CA. However, the created virtual array is not a filled ULA (*i.e.*, it has holes) [10], which will leads to other problems in the following DOA estimation process. Furthermore, when constructing a virtual array from the covariance matrix of the received data, the equivalent sources of the virtual array are considered as fully coherent sources. A spatial smoothing based MUSIC algorithm may be employed to de-correlate the sources [7], [10] and then to estimate the DOAs. However, since spatial smoothing based methods are usually only applicable to ULAs [7], [16], only the ULA part of the virtual array generated from a coprime array may be utilized to perform the DOA estimation. This limitation leads to a reduction in both the DOF and the aperture of the virtual array [10], [15].

B. ALGORITHMS FOR UNDERDETERMINED DOA ESTIMATION

A diversity of algorithms [4], [7], [9], [10], [16]–[19] have been proposed to resolve more sources than sensors using the virtual array derived from a non-uniform linear array, *i.e.*, to solve the underdetermined DOA estimation problem. One representative approach is the spatial smoothing MUSIC (SS-MUSIC) algorithm [7], [9], [16]. A disadvantage of this approach is that not all the elements of the virtual array are used when performing DOA estimation, which may result in a reduction of the signal to noise ratio (SNR). Another representative approach is the sparse signal reconstruction method that takes advantage of the fact that the signal spectra are sparse [10], [17]–[19]. However, algorithms used to implement this approach typically suffer from heavy computational workload.

C. CONTRIBUTIONS OF THIS PAPER

We first summarize the challenges in the array design and in the DOA estimation algorithm.

1) No closed-form expressions for the sensor positions and for the number of achievable DOF in an MRA.
2) Mutual coupling is a considerable problem in an NA.
3) The virtual array generated from a CA is not a filled ULA.
4) Algorithms for the underdetermined DOA estimation are not efficient.

Bearing the above concerns in mind, in this paper we propose a unified array geometry named generalized nested subarray (GNSA) with desired array properties and develop a new algorithm for the underdetermined DOA estimation based upon the proposed GNSA. The contributions of this paper are threefold.

{A.} The proposed GNSA is composed of multiple identical subarrays. Each subarray of the GNSA can be an MRA, a (super) nested array [7], [20], a ULA, or any other linear arrays that have hole-free DCAs. The positions of these subarrays also follow a linear array configuration. By properly designing the inter-subarray spacings, we can obtain a virtual array of this GNSA being a hole-free (filled) ULA. Following our GNSA design methodology, a class of new arrays can be constructed due to the variety of existing linear arrays that have hole-free DCAs. In particular, when the subarray is an MRA and its sensors' positions follow an MRA configuration, the resulting GNSA becomes a nested MRA (NMRA) [11]. Therefore, the NMRA is one special example of our proposed GNSA. Note that the requirement of hole-free DCA is an important constraint for the subsequent DOA estimation. Although it is possible that the nested array might have lower mutual coupling, larger aperture, and more DOFs than our proposed GNSA when the antennas in the nested array are placed in multiple levels, the resulting DCA of the nested array is, unfortunately, not a hole-free ULA, which will cause difficulties in the spatial smoothing based DOA estimation. Furthermore, since the constituent subarrays in the GNSA are identical, the GNSA has noticeable advantages of low cost, relatively simple structure, and easy extension to an array with a very large aperture, and is thus suitable for a wide variety of real-world applications.

{B.} We provide a detailed theoretical analysis on the properties of a GNSA constructed by two subarrays called `Subarray A` and `Subarray B`. Four propositions

TABLE 1. Abbreviations used in the paper.

DCA	Difference CoArray
DOA	Direction Of Arrival
DOF	Degree Of Freedom
GNSA	Generalized Nested SubArray
MRA	Minimum Redundancy Array
ULA	Uniform Linear Array
NMRA	Nested Minimum Redundancy Array
MUSIC	MUltiple SIgnal Classification
ESPRIT	Estimation of Signal Parameters via Rotational Invariance Technique
NA	Nested Array
CA	Coprime Array
SS-MUSIC	Spatial Smoothing MUSIC
SNR	Signal to Noise Ratio
EVD	EigenValue Decomposition
RMSE	Root-Mean-Square-Error
CACIS	CA with Compressed Inter-element Spacing

are presented with proofs to reveal the intrinsic relationships between the GNSA and its components. Based upon these propositions, we analyze the characteristics of different GNSA geometries and compare the GNSA with the MRA, the nested array, and the coprime array using the NMRA as a representative example.

{C.} We propose a new estimation algorithm for the underdetermined DOA estimation using the proposed GNSA. In the algorithm, we introduce a dimension reduction matrix to exploit the data of all virtual elements, and then construct a Toeplitz matrix of the observed data instead of the spatial smoothing operation to decorrelate the equivalent coherent sources. Following this, we apply the root-MUSIC method to avoid the costly angle grid search. Numerical simulations demonstrate that the proposed algorithm can achieve a higher performance than the popular SS-MUSIC algorithm with a lower computational cost.

D. NOTATIONS AND ABBREVIATIONS

Throughout the paper, matrices and vectors are represented by capital letters and lower case letters in boldface, respectively. Superscript $(\cdot)^T$, $(\cdot)^*$ and $(\cdot)^H$ respectively denote the transpose, the conjugate and the conjugate transpose of a matrix or a vector. Statistical expectation is denoted by $E(\cdot)$, and vec$(\cdot)$ is the vectorization operation that stacks all columns of a matrix into a vector. Table 1 summaries the abbreviations used in the paper.

E. ORGANIZATION OF THIS PAPER

The rest of the paper is organized as follows. The signal model is presented in Section II. The proposed array geometry and its properties are developed in Section III, and the array characteristics of the GNSA with different array geometries are described in Section IV. In Section V, we use the NMRA as the representative to compare its characteristics with the nested array and the coprime array. In Section VI, the DOA estimation algorithm is developed for the proposed array.

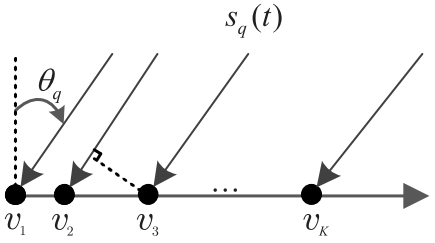

FIGURE 1. Array geometry (normalized by d) for DOA estimation.

Section VII presents numerical examples. Section VIII concludes the paper.

II. SIGNAL MODEL

Consider a K-element linear antenna array with sensors located at

$$\mathbf{v} = [v_1, v_2, \cdots, v_K]d, \tag{1}$$

where $\{v_i\}_{i=1}^K$ are integers, and d is the unit inter-element spacing, usually equal to a half wavelength of the incident signal. Let Q uncorrelated narrow-band sources impinge on the array from directions $\{\theta_q,\ q = 1, 2, \cdots, Q\}$ as shown in Fig. 1. A steering vector is the array response to a unit power source at angle θ,

$$\mathbf{a}(\theta) = \left[e^{j\kappa v_1 \sin\theta}, e^{j\kappa v_2 \sin\theta}, \cdots, e^{j\kappa v_K \sin\theta}\right]^T, \tag{2}$$

where $\kappa = 2\pi d/\lambda$, and λ is the signal wavelength.

The data received by the array can be expressed as

$$\mathbf{x}(t) = \mathbf{A}\mathbf{s}(t) + \mathbf{n}(t), \quad t = 1, \cdots, T, \tag{3}$$

where $\mathbf{A} = \left[\mathbf{a}(\theta_1), \mathbf{a}(\theta_2), \cdots, \mathbf{a}(\theta_Q)\right]$ is the array manifold matrix and T is the number of snapshots. The source signals $\mathbf{s}(t) = \left[s_1(t), s_2(t), \cdots, s_Q(t)\right]^T$ are assumed unknown, but each source $s_q(t)$ is assumed to follow a complex Gaussian distribution $\mathcal{CN}(0, \sigma_q^2)$ with zero mean and variance σ_q^2. These signals are assumed to be mutually independent and uncorrelated over time. The components of the noise vector $\mathbf{n}(t)$ are assumed to be independent and identically distributed (i.i.d.) additive white Gaussian noise with zero mean and variance σ_n^2, and are independent from the sources. The covariance matrix of the received data $\mathbf{x}(t)$ can be expressed as

$$\begin{aligned}\mathbf{R}_{\mathbf{xx}} &= E[\mathbf{x}\mathbf{x}^H] = \mathbf{A}\mathbf{R}_{\mathbf{ss}}\mathbf{A}^H + \sigma_n^2\mathbf{I}_K \\ &= \sum_{q=1}^{Q} \sigma_q^2 \mathbf{a}(\theta_q)\mathbf{a}^H(\theta_q) + \sigma_n^2\mathbf{I}_K,\end{aligned} \tag{4}$$

where $\mathbf{R}_{\mathbf{ss}} = E[\mathbf{s}\mathbf{s}^H]$ is a $Q \times Q$ diagonal matrix with diagonal elements $\{\sigma_1^2, \sigma_2^2, \cdots, \sigma_Q^2\}$, and $\mathbf{I}_K$ is a $K \times K$ identity matrix with the (m, l)-th element denoted as I_{ml}. It should be noted that $I_{ml} = 1$ when $m = l$, and $I_{ml} = 0$ otherwise. In order to exploit the information implied in the covariance matrix,

we examine its (m, l)-th element

$$R_{ml} = \sum_{q=1}^{Q} \sigma_q^2 e^{j\kappa(v_m - v_l)\sin\theta_q} + \sigma_n^2 I_{ml} = \mathbf{b}_{ml}^T(\theta)\mathbf{c} + \sigma_n^2 I_{ml}, \quad 1 \le m, l \le K, \tag{5}$$

where $\mathbf{b}_{ml}(\theta) = \left[e^{j\kappa(v_m - v_l)\sin\theta_1}, \cdots, e^{j\kappa(v_m - v_l)\sin\theta_Q}\right]^T$, $\mathbf{c} = \left[\sigma_1^2, \sigma_2^2, \cdots, \sigma_Q^2\right]^T$. From (5), the covariance R_{ml} may be interpreted as an aggregated signal received from all sources observed at a virtual element located at $(v_m - v_l)d$. By vectorizing matrix $\mathbf{R_{xx}}$, we obtain a $K^2 \times 1$ vector

$$\widetilde{\mathbf{z}} = \mathrm{vec}(\mathbf{R_{xx}}) = \mathbf{B}\mathbf{c} + \sigma_n^2 \mathbf{1}_n, \tag{6}$$

where

- $$\mathbf{B} = \left[\mathbf{a}^*(\theta_1) \otimes \mathbf{a}(\theta_1), \cdots, \mathbf{a}^*(\theta_Q) \otimes \mathbf{a}(\theta_Q)\right]^T = \left[\mathbf{b}(\theta_1), \mathbf{b}(\theta_2), \cdots, \mathbf{b}(\theta_Q)\right] \in \mathbb{C}^{K^2 \times Q}, \tag{7}$$
  with symbol $\otimes$ standing for the Kronecker product;
- $\mathbf{1}_n = \left[\mathbf{e}_1^T, \mathbf{e}_2^T, \cdots, \mathbf{e}_K^T\right]^T$, with $\mathbf{e}_i$ denoting a vector of all zeros, except the i-th element, which is equal to one;
- $\mathbf{c}$ is interpreted as an equivalent source signal vector in the virtual array.

However, it should be noted that the vector $\mathbf{c}$ only contains the powers of the actual sources without their phase information. The rank of its autocorrelation matrix is one, and hence these equivalent sources are considered fully coherent sources to the virtual array.

From (5) and (6), we observe that the vector $\widetilde{\mathbf{z}}$ is equivalent to the data received by a *virtual array* with elements located at the location set

$$\mathbb{V} = \{(v_m - v_l)d, m, l = 1, 2, \cdots, K\}. \tag{8}$$

In this location set $\mathbb{V}$ of the virtual array, there are in total K^2 elements, but some locations may be repeated. More specifically, there may exist multiple pairs of $\{v_m, v_l\}_{m,l=1}^K$ for which $(v_m - v_l)$ are the same. In this case, multiple virtual elements are associated with the same virtual sensor location. We refer to the repeated elements as *redundancies*. The number of redundancies in a virtual array is determined by the structure of the original array. A higher redundancy implies fewer distinct elements in $\mathbb{V}$. The locations of a virtual array are symmetric due to the fact that for any $p_{ml} = (v_m - v_l)d$ in the location set $\mathbb{V}$ in (8), $-p_{ml} = (v_l - v_m)d$ is also in the set $\mathbb{V}$.

We define the virtual array that has sensors located at distinct elements of $\mathbb{V}$, as a *difference coarray (DCA)* of the original array [7]. It should be pointed out that in the location set of the DCA, denoted by $\mathbb{D}$, we have removed all repeated elements in $\mathbb{V}$. Therefore, the number of elements in the DCA is equal to the number of DOF achieved by the virtual array, denoted by f_V, and $f_V < K^2$. If the original array is properly designed, f_V can be larger than the number of physical sensors. Therefore, it is possible to resolve more sources than the number of physical sensors by using a part of or the entire DCA instead of the original array to perform DOA estimation.

When designing an array for which it is possible to resolve more sources than sensors, the following features are desired:

(*a*) A large number of DOFs and a large aperture, which means low redundancies in the virtual array,
(*b*) A closed-form expression for sensor positions and the number of achievable DOF,
(*c*) A DCA that is a hole-free ULA, and
(*d*) A configuration that reduces mutual coupling by preventing elements from being too close to each other.

The proposed GNSA array geometry, especially the NMRA, described in next section meets all these design criteria.

III. PROPOSED GENERALIZED NESTED SUBARRAY (GNSA)

A. ARRAY GEOMETRY

The proposed array is composed of N identical subarrays, denoted by `Subarray A`, and the locations of these `Subarray A` follow the geometry of another subarray denoted by `Subarray B`.

- `Subarray A`: Each subarray has M sensors with locations specified by the vector
$$\mathbf{u}_M = [m_1, m_2, \cdots, m_M]\, d, \tag{9}$$
where d is the unit inter-element spacing, $\{m_i\}_{i=1}^M$ are integers. Without loss of generality, we choose $m_1 = 0$. Each of the subarrays constituting the GNSA is a linear array, such as an MRA, a ULA, or a nested array with two levels, whose difference coarray is a hole-free ULA.
- `Subarray B`: It has N elements, where N may or may not be equal to M. Let the element locations in `Subarray B` be
$$\mathbf{u}_N = [n_1, n_2, \cdots, n_N]\, D, \tag{10}$$
where $\{n_i\}_{i=1}^N$ are integers, $n_1 = 0$, and $D > m_M \cdot d$.

As mentioned earlier, we now combine these two arrays by placing a `Subarray A` at each element location of `Subarray B`. Then the positions of all sensors form a cross summation set

$$\mathbb{S} = \left\{n_j \cdot D + m_i \cdot d, 1 \le j \le N, 1 \le i \le M\right\}. \tag{11}$$

Let $\oplus$ denote the cross summation of every element in $\mathbf{u}_N$ and every element in $\mathbf{u}_M$. In this way the sensor positions of the entire array may be expressed by the vector

$$\mathbf{v} = \mathbf{u}_N \oplus \mathbf{u}_M. \tag{12}$$

This is the *unified* array geometry proposed in our paper. Note that the nesting method embodied in (12) between two linear arrays is different from the nested array introduced in [7], which is a union of two or more uniform linear subarrays.

Owing to the fact that `Subarray B` and `Subarray A` can be any linear array with a hole-free DCA, there are many combinations of the array geometries. We use the form

TABLE 2. Parameters of GNSA and its subarrays.

	Sensor number	Aperture length	Location set of DCA	number of DOF
Subarray A	M	$l_A \cdot d$	$\mathbb{D}_A$	f_A
Subarray B	N	$l_B \cdot d$	$\mathbb{D}_B$	f_B
GNSA	MN	$(f_A l_B + l_A)d$	$\mathbb{D}_B \oplus \mathbb{D}_A$	$f_A f_B$

"Subarray B + Subarray A" to denote the specific array geometry. For example, "MRA + MRA" means that Subarray B and Subarray A are both MRAs, "MRA + ULA" means that Subarray B is an MRA and Subarray A is a ULA, *etc*.

Fig. 2 depicts an example of the proposed array geometry when Subarray A and Subarray B are both MRAs. With $M = 4$ and $N = 3$, the GNSA has $MN = 12$ sensors. Subarray A, Subarray B, the GNSA and its DCA are shown in Fig. 2, with $D = 13d$. We can see that the aperture length of the GNSA is $45d$, and the DCA is a hole-free ULA with $2 \times 45 + 1 = 91$ elements. Hence the number of DOF associated with the DCA is 91. Note that if $D > 13d$, there will be holes in the DCA, which may cause difficulties with spatial smoothing based DOA estimation. On the contrary, $D < 13d$ will result in some additional redundant elements in the virtual array. Therefore it is important to choose a proper spacing D in the GNSA. The following properties establish the optimum value of the spacing D, the aperture of the original array and the number of the DOF in the DCA associated with the GNSA.

B. PROPERTIES OF GNSA

Our design assumes the structures of Subarray A and Subarray B are known. We denote the parameters of the two subarrays in Table 2. Next we derive the properties of a GNSA using the parameters of its components, Subarray A and Subarray B.

Proposition 1: The location set $\mathbb{D}_V$ of the DCA associated with a GNSA is obtained by the cross summation of location sets $\mathbb{D}_B$ and $\mathbb{D}_A$, that is

$$\mathbb{D}_V = \mathbb{D}_B \oplus \mathbb{D}_A. \tag{13}$$

Proof: The proof is provided in Appendix A. □

This proposition reveals the relation between the DCA of a GNSA and the DCAs of its components, Subarray B and Subarray A. According to proposition 1, the locations of the DCA of a larger GNSA may be calculated using the locations of the DCAs of the constituent two subarrays. Proposition 1 also inspires us to compute the aperture length and the number of DOF of the GNSA using parameters of the Subarrays A and B. The following proposition specifies the GNSA.

Proposition 2: If the inter-subarray spacing $D = f_A \cdot d$, the following properties hold for the GNSA constructed according to (12)*:*

(a) *The virtual array of the GNSA is a hole-free ULA with the largest possible aperture.*
(b) *The aperture length of the GNSA is $l_V \cdot d = (f_A \cdot l_B + l_A)\, d$.*
(c) *The aperture length of the DCA is $f_V \cdot d = (2l_V + 1)d$.*
(d) *The number of DOF in the DCA of the GNSA is*

$$f_V = f_A \cdot f_B. \tag{14}$$

Proof: The proof is provided in Appendix B. □

In order to analyze the characteristics of the virtual array of a GNSA, we define a weight function $\mathbf{w}(k)$ to denote the number of times that kd, where $-l_V < k < l_V$, appears in the location set $\mathbb{V}$. We use the following proposition to describe the characteristic of the weight function of a GNSA.

Proposition 3: Assume that the weight function of Subarray A is $\mathbf{w}_A \in \mathbb{R}^{f_A}$, and the weight function of Subarray B is $\mathbf{w}_B \in \mathbb{R}^{f_B}$. The weight function $\mathbf{w}_V$ of the GNSA can be calculated by the Kronecker product of $\mathbf{w}_B$ and $\mathbf{w}_A$, that is

$$\mathbf{w}_V = \mathbf{w}_B \otimes \mathbf{w}_A. \tag{15}$$

Proof: The proof is provided in Appendix C. □

Proposition 4: For the GNSA $\mathbf{v}$ defined in (12)*, if we exchange Subarray A and Subarray B and their inter-element spacing, that is using M identical N-sensor subarrays to form a new GNSA $\mathbf{v}'$ and the unit spacing D' among the subarrays becomes $f_B \cdot d$, then the aperture length of the GNSA $\mathbf{v}'$ and the number of DOF in its DCA will keep the same as those of $\mathbf{v}$.*

Proof: The proof for the DOF is obvious using the commutative law of multiplication because both numbers of the DOF associated with the two GNSAs are equal to $f_A \cdot f_B$.

Because the DCAs of Subarray A and Subarray B are hole-free ULAs and have the symmetric property, we can obtain the relations $f_A = 2l_A + 1$, $f_B = 2l_B + 1$ for Subarray A and Subarray B, respectively. From proposition 2 we know that the aperture length of the GNSA $\mathbf{v}$ constructed by N identical M-sensor subarrays is

$$\begin{aligned} l_V \cdot d &= (f_A \cdot l_B + l_A)d \\ &= [(2l_A + 1)\, l_B + l_A]\, d \\ &= (2l_A \cdot l_B + l_B + l_A)\, d. \end{aligned} \tag{16}$$

The aperture length of the new GNSA $\mathbf{v}'$ constructed by M identical N-sensor subarrays can be obtained by

$$\begin{aligned} l_{V'} \cdot d &= (f_B \cdot l_A + l_B)d \\ &= [(2l_B + 1)\, l_A + l_B]\, d \\ &= (2l_B \cdot l_A + l_A + l_B)\, d. \end{aligned} \tag{17}$$

Thus $l_{V'} = l_V$. □

Proposition 4 implies that there exist two array manifolds to construct a GNSA for a given number of M and N. Therefore we may consider some other factors, such as mutual coupling, peak side lobe level, in addition to the aperture and the DOF to select one of the manifolds.

In the following, we will use these properties to analyze the GNSA with some examples.

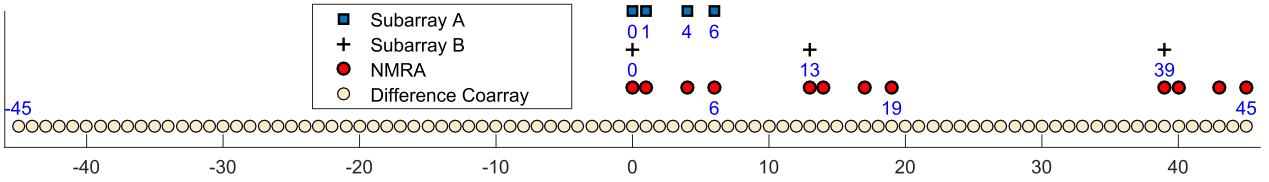

FIGURE 2. An example geometry of GNSA consists of 3 identical 4-element minimum redundancy subarrays, in which $D = 13d$.

TABLE 3. Parameter comparisons of different GNSA geometries.

Array geometries	Inter-subarray spacing($*d$)	Array Aperture ($*d$)	Maximum Number of DOF
MRA+MRA[1]	f_{MRA}	$[N(N-1)/2 - N_R/2]f_{MRA} + M(M-1)/2 - M_R/2$	$[N(N-1)+1-N_R]f_{MRA}$
ULA+MRA	f_{MRA}[2]	$(N-1)f_{MRA} + M(M-1)/2 - M_R/2$	$(2N-1)f_{MRA}$
NA+MRA	f_{MRA}	$l_{NA} \cdot f_{MRA} + M(M-1)/2 - M_R/2$	$(2l_{NA}+1)f_{MRA}$
MRA+NA	f_{NA}	$[N(N-1)/2 - N_R/2]f_{NA} + (f_{NA}-1)/2$	$[N(N-1)+1-N_R]f_{NA}$
ULA+NA	f_{NA}[1]	$(N-1)f_{NA} + (f_{NA}-1)/2$	$(2N-1)f_{NA}$
NA+NA	f_{NA}	$l_{NA} \cdot f_{NA} + (f_{NA}-1)/2$	$(2l_{NA}+1)f_{NA}$
MRA+ULA	$(2M-1)$	$[N(N-1)/2 - N_R/2](2M-1) + M - 1$	$[N(N-1)+1-N_R](2M-1)$
ULA+ULA	$2M-1$	$(N-1)(2M-1) + M - 1$	$(2N-1)(2M-1)$
NA+ULA	$(2M-1)$	l_{NA}[4]$\cdot(2M-1) + M - 1$	$(2l_{NA}+1)(2M-1)$

[1] We use the form "`Subarray B` + `Subarray A`" to express the array geometries, where `Subarray B` has N sensors and `Subarray A` has M sensors.
[2] $f_{MRA} = M^2 - M + 1 - M_R$.
[3] $f_{NA} = \begin{cases} M^2/2 + M - 1 \text{ , if } M \text{ is even} \\ (M+1)^2/2 - 1 \text{ , if } M \text{ is odd} \end{cases}$.
[4] $l_{NA} = \begin{cases} N^2/4 + N/2 - 1 \text{ , if } N \text{ is even} \\ (N+1)^2/4 - 1 \text{ , if } N \text{ is odd} \end{cases}$.

IV. CHARACTERISTICS OF NESTED SUBARRAY WITH DIFFERENT ARRAY GEOMETRIES

In the proposed unified array geometry, the subarray can be an MRA, a nested array, a ULA, or any other linear arrays with hole-free DCAs. Therefore, there are multiple combinations of array geometries. In this section, we will analyze the characteristics of the GNSA with different array geometries using the properties presented in Section III-B.

A. MRA + MRA

When `Subarray B` and `Subarray A` are both MRAs, the nested subarray can be treated as an MRA of MRA subarrays. This array has the largest aperture, maximum number of DOF and lowest redundancies among these combinations for a fixed number of physical sensors. We also name this array as *Nested MRA* (NMRA) [11]. This array can be used to construct an MRA with a large number of antennas. The numbers of DOF of `Subarray A` and `Subarray B` can be expressed respectively by [12]

$$\begin{aligned} f_A &= M^2 - M + 1 - M_R, \\ f_B &= N^2 - N + 1 - N_R, \end{aligned} \tag{18}$$

where M_R and N_R are the number of redundancies for an M-sensor MRA and an N-sensor MRA, respectively. Substituting (18) into (14), we obtain

$$\begin{aligned} f_V &= f_A \cdot f_B \\ &= \left(M^2 - M + 1 - M_R\right)\left(N^2 - N + 1 - N_R\right). \end{aligned} \tag{19}$$

Therefore it can be concluded that an *NMRA can provide $\mathcal{O}(M^2N^2)$ DOFs using only MN physical sensors* when `Subarray A` and `Subarray B` are both MRAs.

Fig. 2 is an illustration of 12-element NMRA. We will compare the characteristics of the NMRA with the MRA, the nested array and the coprime array in Section V.

B. ULA (MRA, NA) + ULA

If `Subarray A` is a ULA, the GNSA is a repetition of multiple ULA subarrays. This kind of array has been widely studied [21]–[23] because the array aperture can be easily extended without causing significant increase in software and hardware costs. However, there is no criteria for the inter-subarray spacing. In our proposed GNSA, we properly design the inter-subarray spacing to form a hole-free DCA, and derive closed-form expressions for the sensor positions and the number of achievable DOF.

For an M-element ULA with unit inter-element spacing d, the aperture length and the number of DOF achieved by its DCA are $(M-1)d$ and $2M-1$, respectively. According to Proposition 2, the inter-subarray spacing is $D = (2M-1)d$ when `Subarray A` is a ULA. Therefore, we can obtain the aperture length of the "ULA + ULA", "MRA + ULA" and "NA + ULA"and their number of DOF using Proposition 2, which are shown in Table 3.

C. NA + NA

If both `Subarray B` and `Subarray A` are nested linear array, we will obtain a nested subarray of "NA + NA". Fig. 3(f) gives an example of "NA + NA", from which we

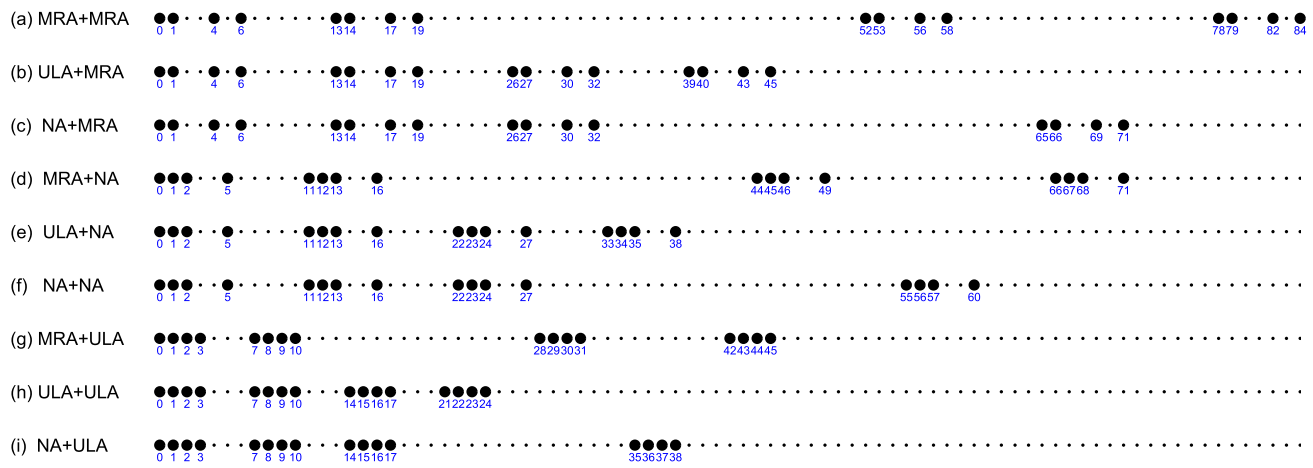

FIGURE 3. Array geometries of GNSA for $N = 4$ and $M = 4$. (a) MRA+MRA. (b) ULA+MRA. (c) NA+MRA. (d) MRA+NA. (e) ULA+NA. (f) NA+NA. (g) MRA+ULA. (h) ULA+ULA. (i) NA+ULA.

can see that the array geometry is composed of several NAs. This geometry is different from the nested array with multiple levels [14] which consists of multiple level ULAs with an increased inter-element spacing in each level. Although the NA with more than two levels can obtain more degrees of freedom, its difference coarray is not a hole-free ULA [7]. Therefore in our paper we will only consider two level nested array whose DCA has no holes, for a fair comparison. The "NA + NA" structure is more suitable for distributed array application owing to its multiple subarray structure.

For a two level nested array with M physical sensors, the maximum number of DOF is [7]

$$f_{NA} = \begin{cases} M^2/2 + M - 1, & \text{if } M \text{ is even;} \\ (M+1)^2/2 - 1, & \text{if } M \text{ is odd.} \end{cases} \tag{20}$$

The aperture length is

$$l_{NA} \cdot d = (f_{NA} - 1) \cdot d/2. \tag{21}$$

Substituting (20) and (21) into Proposition 2, we can obtain the corresponding parameters of the "NA + NA" shown in Table 3.

D. OTHER COMBINATIONS

In addition to the above three array geometries, there are some other combinations such as "MRA + NA", "ULA + MRA", "NA + MRA" and "ULA + NA", *etc*. The number of achievable DOF and the aperture length for different array geometries can be obtained using Proposition 2 and relevant expressions from [7], [8], and [10], which are summarized in Table 3. Furthermore, the array configurations can be extended to other combinations when the subarrays are other linear array geometries with hole-free DCAs, *e.g.* super nested array (SNA) [20]. We can form some other new array geometries, e.g. "MRA + SNA", "ULA + SNA", "SNA + MRA" and so on.

TABLE 4. Array configuration parameters.

Number of sensors (K)	9	12	16	18	20	24	27	30	32	36
M_1 for nested array	4	6	8	9	10	12	13	15	16	18
N_1 for nested array	5	6	8	9	10	12	14	15	16	18
N_2 for CACIS	7	7	9	11	11	11	13	15	17	17
M_2 for CACIS	3	6	8	8	10	14	15	16	16	20
p[1] for CACIS	1	3	4	4	5	7	5	8	8	10
N for GNSA	3	3	4	3	4	4	3	5	4	4
M for GNSA	3	4	4	6	5	6	9	6	8	9

[1] p is a factor of M_2.

Fig. 3 illustrates the array geometries of GNSA for $M = N = 4$. The inter-subarray spacing is chosen to form a hole-free DCA. From Fig. 3, we can see that the "MRA + MRA" structure has the largest aperture $84d$, the "ULA + ULA" structure has the smallest aperture $24d$, and the apertures of other arrays are in between the former two array structures.

Next, we compare the number of achieved DOF from the DCA of the GNSA. Let the total number of sensors be some integers from 9 to 36, and choose the optimal number of sensors in the subarrays of different array geometries as listed in Table 4. The number of achievable DOF and the aperture length for different array geometries can be obtained using the equations in Table 3. The comparison results are shown in Fig. 4. We can see that the "MRA + MRA" structure can achieve the maximum number of DOF, the "ULA + ULA" structure has the minimum number of DOF, and the numbers of DOF from other array geometries are somewhere in between. This feature gives us more options to choose an appropriate array geometry from these combinations based on practical applications.

The difference between the proposed GNSA and the existing non-uniform linear array will be discussed in the next section.

V. COMPARE NMRA WITH OTHER ARRAY GEOMETRIES

In this section, we use the NMRA as an example of the proposed GNSA to compare its characteristics with other

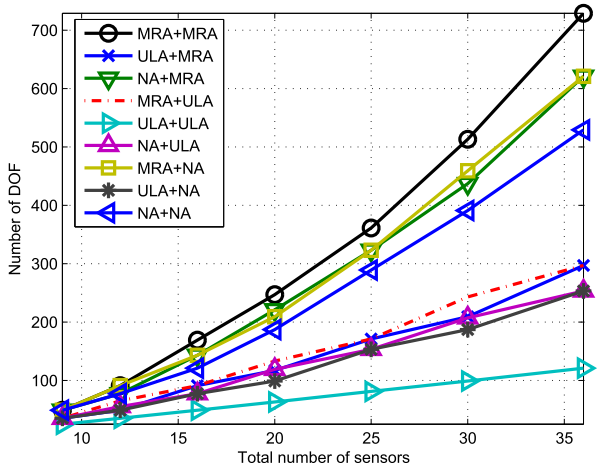

FIGURE 4. DOF comparisons of different GNSA geometries with total number of sensors.

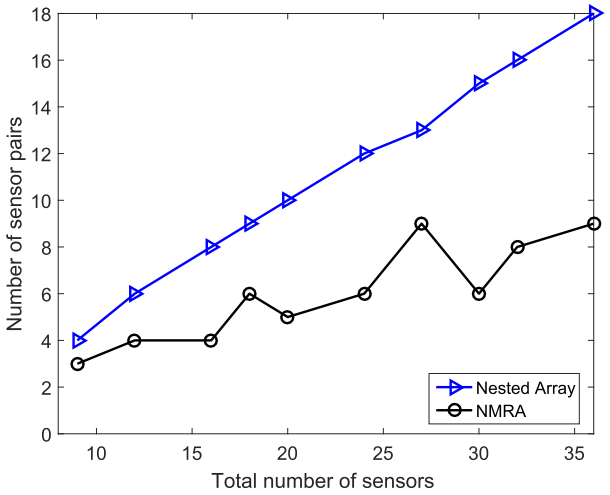

FIGURE 5. Number of sensor pairs, which are separated by d, comparison of the nested array with two ULA subarrays and the NMRA versus total number of sensors.

arrays, including the MRA, the nested array and the coprime array.

1) Since the MRA [8] is optimized to produce the largest DCA under the constraint that the DCA is a hole-free ULA, the proposed NMRA will not produce more DOFs than an MRA with the same number of physical sensors. However, the optimal design of an MRA is usually analytically intractable, obtainable only by exhaustive search or complicated algorithms [9]. By contrast, the NMRA uses cross summation of two MRA subarrays to generate a new array, which is easy to construct based on the known MRA. The sensor positions and the number of DOF can be obtained using (12) and (19) when these parameters of the MRA subarrays are known. Thus, given an N-element MRA, it is possible to design a much larger N^2-element NMRA.

2) The nested array [7] is the union of two ULA subarrays, where the first ULA has M_1 sensors with inter-element spacing d, the other has N_1 sensors with inter-element spacing $d_2 = (M_1+1)d$. One shortcoming of the nested array is the possible mutual coupling problem caused by the sensor pairs separated by $d = \lambda/2$ [16]. When maximizing the total DOF, the optimal values of M_1 and N_1 in the nested array are integers around $K/2$ under the constraint of fixed K sensors [7]. Thus there are $M_1 \approx K/2$ pair of sensors separated by d for a K-element nested array.

There are a small number of sensor pairs spaced by d in an MRA, *e.g.*, four at most for MRAs with less than 17 sensors [12]. The NMRA is composed of multiple MRA subarrays and thus an NMRA may have fewer closely spaced elements than the nested array. Let m denote the number of sensor pairs, which are separated by d in an M-element MRA. Then the NMRA constructed by N identical M-element minimum redundancy subarrays has mN pairs of sensors separated by d. We plot the number of sensor pairs separated by d in the nested array (NA) and the NMRA with some total number of physical sensors K in Fig. 5. We see that the number of sensor pairs M_1 in the nested array is proportional to K, and these numbers are larger than the number of sensor pairs in the NMRA. Thereby the NMRA is subject to lower mutual coupling than the nested array with same number of sensors. At the same time, the NMRA has a larger aperture and more DOFs than the nested array which will be shown in Fig. 6 and is discussed next.

The nested array with more than two ULA subarrays [14] has less mutual coupling by increasing the inter-element spacing of last few subarrays. But the virtual array generated from the nested array is not a hole-free ULA, which may cause difficulties with spatial smoothing based DOA estimation.

3) The coprime array [9], [10] is constructed by two ULA subarrays with M_2, N_2 elements respectively, where M_2, N_2 are coprime integers. The corresponding inter-element spacings in both ULAs are N_2d and M_2d, respectively. The coprime array allows adjacent elements to be spaced farther apart, which is helpful for reducing the mutual coupling between elements. However the DCA generated from a coprime array is not a hole-free ULA. The NMRA can avoid holes by setting a proper unit spacing D in `Subarray B`.

Next, we compare the aperture length and the number of DOF of the four array geometries mentioned above. We use the coprime array with compressed inter-element spacing (CACIS) in [10], which is an extended coprime array with fewer holes, as the representative of the coprime array. Let the total number of sensors be some integers from 9 to 36, and choose the optimal number of sensors in the subarrays of different array geometries as listed in Table 4. The number of achievable DOF and the aperture length for different array geometries can be obtained using Proposition 2 and relevant expressions from [7], [10]. The comparison results are shown in Fig. 6, in which the table at the top-left corner lists the first six corresponding values. We show that our proposed NMRAs have the highest DOF and largest aperture except the MRAs smaller than 17 sensors. However, no such MRAs

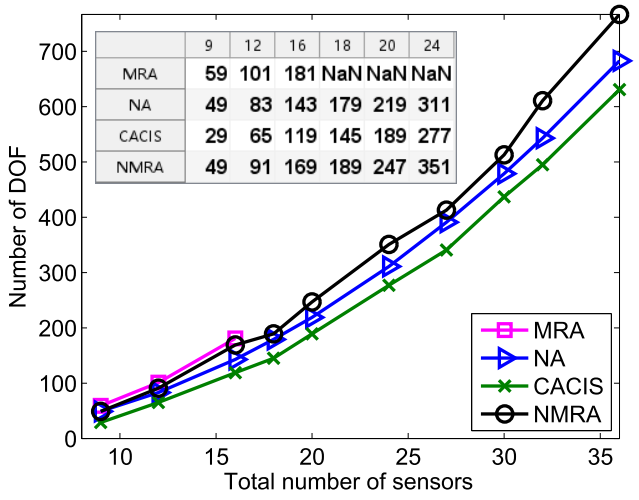

	9	12	16	18	20	24
MRA	59	101	181	NaN	NaN	NaN
NA	49	83	143	179	219	311
CACIS	29	65	119	145	189	277
NMRA	49	91	169	189	247	351

(a)

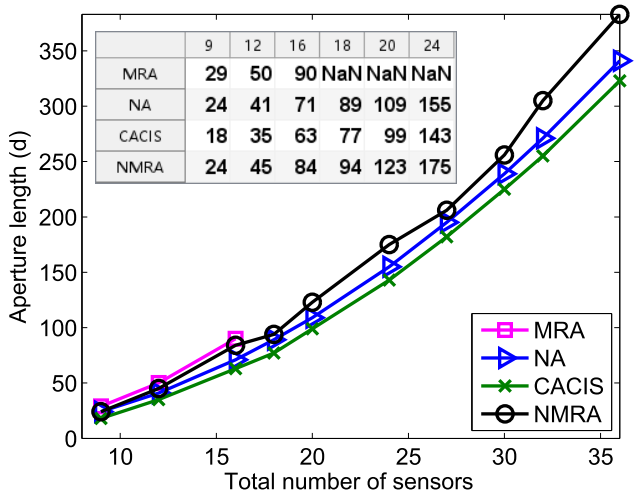

	9	12	16	18	20	24
MRA	29	50	90	NaN	NaN	NaN
NA	24	41	71	89	109	155
CACIS	18	35	63	77	99	143
NMRA	24	45	84	94	123	175

(b)

FIGURE 6. Parameter comparisons of different array geometries with total number of sensors, in which the table at the top-left corner lists the first 6 corresponding values for clear viewing and NA is short for nested array. When the number of sensors is larger than 17, there are no such known MRAs and no expression for their parameters, shown by 'NaN' in the corresponding cell. (a) The number of DOF comparison. (b) Aperture length comparison in the unit of the spacing d.

with more than 17 sensors have been reported in the literature and hence their parameters are shown as 'NaN' in the corresponding table. Although the CACIS has the advantage of reducing mutual coupling, it has fewer DOF and smaller aperture than the nested array and the NMRA.

To summarize, the proposed NMRA satisfies all of the four features required for an array to resolve more sources than the number of sensors, which are listed in Section II. The sensor positions, aperture length and the number of the DOF of an NMRA can be predicted using the parameters of the known MRA subarrays. The DCA can be a hole-free ULA when $D = f_A \cdot d$. The NMRA has more DOFs and larger aperture than the nested array and the CACIS, with the same number of physical sensors. Moreover, the NMRA has lower mutual coupling than the nested array with two levels.

VI. DOA ESTIMATION ALGORITHM

In this section we develop DOA estimation algorithms applied to the virtual array of a GNSA to resolve more sources than sensors. Recall the equivalent source signal vector $\mathbf{c} = \left[\sigma_1^2, \sigma_2^2, \cdots, \sigma_Q^2\right]^T$ in (6), which is composed of the powers of the actual sources. All elements in $\mathbf{c}$ are real values, and hence the rank of its autocorrelation matrix is one. The equivalent sources are considered fully coherent sources to the virtual array. The traditional subspace-based DOA estimation algorithms, such as MUSIC and ESPRIT, cannot be directly applied to the virtual array to estimate DOAs. Various algorithms [7], [9], [10], [18], [19] have been proposed to decorrelate the sources and to perform DOA estimation. However, as we pointed out earlier in Section I, the SS-MUSIC algorithm [7], [9] does not use all elements of the virtual array, which may degrade the performance of DOA estimation. In addition, sparse signal reconstruction based algorithm [18], [19] usually requires a heavy computational workload because it is based on the signal spectra sparsity which is typically divided into numerous small grids to maintain the accuracy. To overcome these limitations, we propose a new DOA estimation algorithm for the virtual array in this section.

First, we obtain the observation data of the DCA by exploiting the data of all virtual elements, instead of removing the repeated ones. Then we impose a Toeplitz structure matrix on the observation data to decorrelate the sources. This Toeplitz matrix is constructed by reshaping the observation data and thus no multiplication is required. Finally, a polynomial root MUSIC algorithm is employed to calculate the DOA, which avoids the angle grid search in the standard spectral MUSIC [1]. The use of the Toeplitz matrix and root-MUSIC algorithm make the computation of our approach more efficient than the SS-MUSIC algorithm [7]. To be more specific, we analyze the computation of both SS-MUSIC and our method in Section VI-D, and the corresponding comparison results are enumerated in Table 5, which shows the superiority of our method clearly.

A. OBSERVATION DATA OF DIFFERENCE COARRAY

Consider a K-element GNSA constructed by (12), and the signal model of its virtual array is given by (6) in Section II. The virtual array of the GNSA has K^2 elements with a steering vector $\mathbf{b}(\theta)$ given by (7). From Proposition 2, we know that the DCA associated with the GNSA is a hole-free ULA with f_V elements located at $[-l_V, l_V]d$, recalling that l_V is the aperture length of the GNSA and $f_V = 2l_V + 1$. Therefore, the steering vector of the DCA, $\mathbf{g}(\theta) \in \mathbb{C}^{f_V \times 1}$ can be expressed as

$$\mathbf{g}(\theta) = \left[e^{j\kappa(-l_V)\sin\theta}, e^{j\kappa(-l_V+1)\sin\theta}, \cdots, e^{j\kappa l_V \sin\theta}\right]^T. \tag{22}$$

The two steering vectors $\mathbf{g}(\theta)$ and $\mathbf{b}(\theta)$ are related by

$$\mathbf{b}(\theta) = \mathbf{E}\mathbf{g}(\theta), \tag{23}$$

where

$$\mathbf{E} = \left[\hat{\mathbf{e}}_{p_1}, \hat{\mathbf{e}}_{p_2}, \cdots, \hat{\mathbf{e}}_{p_{K^2}}\right]^T \in \mathbb{C}^{K^2 \times f_V}, \tag{24}$$

where $\hat{\mathbf{e}}_{p_l}$ is a $f_V \times 1$ vector of all zeros except a 1 at the p_l-th position, and $p_l = v_i - v_j + (f_V + 1)/2$, with $l = (j-1)K + i,\ i, j = 1, 2, \cdots, K$. Taking the GNSA in Fig. 2 as an example. The virtual array has $K^2 = 144$ elements, and the DCA has $f_V = 91$ elements. Then $\mathbf{E}$ is the 144×91 matrix as shown in (25) at the bottom of this page.

The location of the k-th virtual element in the virtual array is mapped to a "1" in the k-th row of $\mathbf{E}$. For example, the positions of the first four virtual elements are $v_i - v_1 = [0, 1, 4, 6]d$, $i = 1, 2, 3, 4$. Hence the positions of "1"s in the first four rows of $\mathbf{E}$ are $v_i - v_1 + (f_V + 1)/2 = [46, 47, 50, 52]$, respectively.

Let $\mathbf{W} = \mathbf{E}^T\mathbf{E}$. We show in Appendix D that $\mathbf{W}$ is a diagonal matrix, and its diagonal elements are equal to the values of the weight function $\mathbf{w}$ defined in Section III-B. Therefore,

$$\mathbf{w} = \text{diag}(\mathbf{W}) = \text{diag}(\mathbf{E}^T\mathbf{E}), \tag{26}$$

where $\text{diag}(\mathbf{W})$ extracts the diagonal elements of $\mathbf{W}$.

Equation (25) shows that there exist several "1"s located at the same column, which correspond to the repeated elements in the location set $\mathbb{V}$. The repeated elements are deleted when performing DOA estimation with the SS-MUSIC algorithm [7], [9], which may lead to a reduction in SNR. Here, we use a reduced dimensional matrix to obtain the observation data of the DCA using the data of all elements of the virtual array. The reduced dimensional matrix is constructed by

$$\mathbf{T} = \mathbf{W}^{-1}\mathbf{E}^T \in \mathbb{C}^{f_V \times K^2}. \tag{27}$$

It can transform $\mathbf{b}(\theta) \in \mathbb{C}^{K^2 \times 1}$ into $\mathbf{g}(\theta) \in \mathbb{C}^{f_V \times 1}$, that is $\mathbf{g}(\theta) = \mathbf{T}\mathbf{b}(\theta)$. Then the observation data at the DCA of the GNSA can be obtained by

$$\begin{aligned} \mathbf{z} &= \mathbf{T}\widetilde{\mathbf{z}} \\ &= \mathbf{T}\mathbf{B}\mathbf{c} + \sigma_n^2\mathbf{T}\mathbf{1}_n \\ &= \mathbf{G}\mathbf{c} + \sigma_n^2\widetilde{\mathbf{e}}, \end{aligned} \tag{28}$$

where $\mathbf{G} = \left[\mathbf{g}(\theta_1), \mathbf{g}(\theta_2), \cdots, \mathbf{g}(\theta_Q)\right] \in \mathbb{C}^{f_V \times Q^2}$ is a manifold matrix, $\widetilde{\mathbf{e}}$ is a $(2l_V + 1) \times 1$ vector of all zeros except a 1 at the $(l_V + 1)$-th position. By $\mathbf{T} = \mathbf{W}^{-1}\mathbf{E}^T$, (28) averages out the amplitudes of the data of the repeated virtual elements.

B. DECORRELATION OF EQUIVALENT SOURCES

As mentioned above, the equivalent sources behave like fully coherent signals in the DCA, and some operation should be performed to decorrelate the signals prior to applying traditional DOA estimation algorithms to the DCA. A common method is to apply a spatial smoothing technique [24], and it is applicable to the GNSA. First let us briefly review the SS-MUSIC algorithm in [7] applied to the DCA of the GNSA.

The DCA $\mathbf{z}$ is divided into $l_V + 1$ overlapping subarrays $\mathbf{z}_{si}$ ($i = 1, 2, \cdots, l_V + 1$, each with $l_V + 1$ elements), where the i-th subarray has sensors located at $\{(-i + 1 + n)d,\ n = 0, 1, \cdots, l_V\}$. Define the covariance matrix of $\mathbf{z}_{si}$ as $\mathbf{R}_i = \mathbf{z}_{si}\mathbf{z}_{si}^H$. Then taking the average of $\mathbf{R}_i$ over i, we get the spatially smoothed matrix

$$\mathbf{R}_{\text{SS}} = \frac{1}{l_V + 1}\sum_{i=1}^{l_V+1}\mathbf{R}_i. \tag{29}$$

If the number of sources Q is less than $l_V + 1$, the rank of matrix $\mathbf{R}_{\text{SS}}$ can be restored [24]. Therefore the MUSIC algorithm [1] can be applied to $\mathbf{R}_{\text{SS}}$ for DOA estimation. It has been shown that the SS-MUSIC algorithm can resolve more sources than sensors, and can achieve a high angular resolution [7]. However it involves the average of several covariance matrices, which implies a high computation cost.

Hereby, we employ a computationally efficient method to decorrelate the signals. We directly use the observation data $\mathbf{z}$ to construct a Toeplitz data matrix $\mathbf{Y}$. It can be proved that $\mathbf{Y}$ is a full rank matrix and it share the same signal subspace with $\mathbf{R}_{\text{SS}}$, that is the coherency problem of the equivalent sources can be solved by $\mathbf{Y}$. Therefore we can directly use $\mathbf{Y}$, instead of the spatially smoothed matrix $\mathbf{R}_{\text{SS}}$, to estimate the signal subspace and noise subspace, and subsequently perform DOA estimation.

$$\mathbf{E} = \begin{array}{c} \\ 1 \\ 2 \\ 3 \\ 4 \\ \vdots \\ 141 \\ 142 \\ 143 \\ 144 \end{array} \begin{array}{c} \begin{array}{cccccccccccccccccc} 1 & \cdots & 40 & 41 & 42 & 43 & 44 & 45 & 46 & 47 & 48 & 49 & 50 & 51 & 52 & \cdots & 91 \end{array} \\ \begin{pmatrix} 0 & \cdots & 0 & 0 & 0 & 0 & 0 & 0 & 1 & 0 & 0 & 0 & 0 & 0 & 0 & \cdots & 0 \\ 0 & \cdots & 0 & 0 & 0 & 0 & 0 & 0 & 0 & 1 & 0 & 0 & 0 & 0 & 0 & \cdots & 0 \\ 0 & \cdots & 0 & 0 & 0 & 0 & 0 & 0 & 0 & 0 & 0 & 0 & 1 & 0 & 0 & \cdots & 0 \\ 0 & \cdots & 0 & 0 & 0 & 0 & 0 & 0 & 0 & 0 & 0 & 0 & 0 & 0 & 1 & \cdots & 0 \\ \vdots & \cdots & & & & & & \ddots & & & & & & & & \cdots & \vdots \\ 0 & \cdots & 1 & 0 & 0 & 0 & 0 & 0 & 0 & 0 & 0 & 0 & 0 & 0 & 0 & \cdots & 0 \\ 0 & \cdots & 0 & 1 & 0 & 0 & 0 & 0 & 0 & 0 & 0 & 0 & 0 & 0 & 0 & \cdots & 0 \\ 0 & \cdots & 0 & 0 & 0 & 0 & 1 & 0 & 0 & 0 & 0 & 0 & 0 & 0 & 0 & \cdots & 0 \\ 0 & \cdots & 0 & 0 & 0 & 0 & 0 & 0 & 1 & 0 & 0 & 0 & 0 & 0 & 0 & \cdots & 0 \end{pmatrix} \end{array} \in \mathbb{C}^{144 \times 91}. \tag{25}$$

The Toeplitz matrix is constructed by

$$\mathbf{Y} = \begin{bmatrix} z_{l_V+1} & z_{l_V} & \cdots & z_1 \\ z_{l_V+2} & z_{l_V+1} & \cdots & z_2 \\ \vdots & \vdots & \vdots & \vdots \\ z_{2l_V+1} & z_{2l_V} & \cdots & z_{l_V+1} \end{bmatrix}, \tag{30}$$

where z_i is the i-th element of $\mathbf{z}$. We state the following theorems about the matrix $\mathbf{Y}$.

Theorem 1: If the number of the sources $Q < l_V + 1$, $\mathbf{Y}$ is a full rank matrix, which is independent of the coherency of the sources.

Proof: The proof is provided in Appendix E. □

From Theorem 1 we know that $\mathbf{Y}$ is a full rank matrix, which has no connection with the coherency of the equivalent sources. Therefore, it is possible to estimate the signal and noise subspace correctly with $\mathbf{Y}$.

Theorem 2: The Toeplitz matrix $\mathbf{Y}$ is Hermitian symmetric and $\mathbf{Y}^2 = (l_V + 1)\mathbf{R}_{SS}$.

A similar conclusion and proof can be found in [7] and [25]. It follows that $\mathbf{Y}$ and $\mathbf{R}_{\mathrm{SS}}$ share the same eigenvectors. Therefore we can use the eigenvalue decomposition (EVD) of $\mathbf{Y}$ to obtain the signal and noise subspace. From this perspective, $\mathbf{Y}$ has the same decorrelation effect as the spatial smoothing step, and the spatial smoothing step can be avoided. Since $\mathbf{Y}$ is constructed by reshaping the elements of $\mathbf{z}$, it does not need multiplication. The computational complexity is reduced when using $\mathbf{Y}$, instead of $\mathbf{R}_{\mathrm{SS}}$, to conduct DOA estimation.

C. ROOTING BASED DOA ESTIMATION

The standard spectral MUSIC algorithm [1] can be directly applied to $\mathbf{Y}$ or $\mathbf{R}_{\mathrm{SS}}$ to perform DOA estimation. However the spectral MUSIC algorithm needs an angle grid search, which leads to a high computational cost especially for a large angle scope and/or a fine angle grid. Here we apply a polynomial rooting method to perform DOA estimation. This method does not need costly angle grid search, and hence reduces computational complexity.

Define the EVD of $\mathbf{Y}$ as

$$\mathbf{Y} = \mathbf{U}_S \Lambda_S \mathbf{U}_S^H + \sigma_n^2 \mathbf{U}_N \mathbf{U}_N^H, \tag{31}$$

where $\Lambda_S = \mathrm{Diag}\{\lambda_1, \lambda_2, \cdots, \lambda_Q\}$ with λ_i $(i = 1, 2, \cdots, Q)$ being the signal eigenvalues, and $\mathbf{U}_S \in \mathbb{C}^{(l_V+1)\times Q}$, $\mathbf{U}_N \in \mathbb{C}^{(l_V+1)\times(l_V+1-Q)}$ are the signal and noise subspace, respectively.

Then the root-MUSIC polynomial [26], [27] is given by

$$f_{\mathrm{MUSIC}}(r) = \mathbf{d}^T(1/r)\mathbf{U}_N\mathbf{U}_N^H\mathbf{d}(r), \tag{32}$$

where $r = e^{j(2\pi/\lambda)d\sin\theta}$, and $\mathbf{d}(r) = \left[1, r, \cdots, r^{l_V}\right]$. By finding the Q roots $r_i (i = 1, 2, \cdots, Q)$ which are closest to the unit circle, we obtain the DOAs of the sources

$$\theta_i = \arcsin\left(\frac{arg(r_i)\lambda}{2\pi d}\right), \tag{33}$$

where $arg(x)$ represents the angle of the complex number x. The procedure of the entire algorithm is shown in Algorithm 1.

Algorithm 1 Proposed DOA Estimation Algorithm

Require: The received data $\mathbf{x}(t) = \mathbf{A}\mathbf{s}(t) + \mathbf{n}(t)$, $t = 1, 2, \cdots, T$, and the source number Q.

1: Compute the covariance matrix $\hat{\mathbf{R}}_{\mathbf{xx}} = \frac{1}{T}\sum_{t=1}^{T}\mathbf{x}(t)\mathbf{x}^H(t)$.
2: Vectorize $\hat{\mathbf{R}}_{\mathbf{xx}}$ to obtain the data vector $\widetilde{\mathbf{z}}$ of the virtual array.
3: Construct the reduced dimensional matrix $\mathbf{T} = (\mathbf{E}^T\mathbf{E})^{-1}\mathbf{E}^T$, and compute the observation data $\mathbf{z} = \mathbf{T}\widetilde{\mathbf{z}}$ of the DCA.
4: Construct the Toeplitz matrix $\mathbf{Y}$ using (30).
5: Perform EVD on $\mathbf{Y}$ to obtain the noise subspace $\mathbf{U}_N$.
6: Construct the root-MUSIC polynomial f_{MUSIC} using (32), and compute its roots.
7: Pick Q roots $r_i (i = 1, 2, \cdots, Q)$ which are closest to the unit circle, and compute the DOAs using (33).

In summary, our proposed algorithm utilizes the data of all virtual elements, a Toeplitz matrix instead of the spatial smoothing operation to decorrelate the equivalent sources, and a root-MUSIC algorithm to avoid costly angle grid search. The new algorithm achieves better DOA estimation performance and reduces computational complexity.

Although the new DOA estimation algorithm is designed for the GNSA, it also works for any non-uniform linear array whose DCA is a hole-free ULA, *e.g.* the MRA [8] and the nested array with two levels [7]. When the new algorithm is applied to a coprime array whose DCA is not a hole-free ULA, the reduced dimensional matrix $\mathbf{T}$ can also be constructed by (27). However, the Toeplitz matrix and the root-MUSIC algorithm can only use the ULA part of the DCA generated by a coprime array.

D. COMPLEXITY ANALYSIS

Our DOA estimation algorithm has advantages of reducing the computational cost. In this subsection we analyze its computational complexity and compare it with the SS-MUSIC algorithm. The DOA estimation algorithms can be divided into the following steps:

1) *Compute covariance matrix $\mathbf{R}_{\mathbf{xx}}$ (4) and construct the data vector $\widetilde{\mathbf{z}}$ (6) of the virtual array.* It needs $\mathcal{O}(K^2T)$ complex multiplications to compute $\mathbf{R}_{\mathbf{xx}}$. Since the data vector of the virtual array can be obtained by vectorizing the covariance matrix, it does not need multiplication. These steps are the same for the two algorithms.

2) *Compute the observation data $\mathbf{z}$ (28) of the DCA.* We use a reduced dimensional matrix $\mathbf{T}$ (27) to compute $\mathbf{z}$. The matrix $\mathbf{T}$ can be determined once the element locations of the original array are given, and every column of $\mathbf{T}$ is a unitary vector. The essence of (28) is to average the amplitudes of

TABLE 5. Complexity comparison.

Algorithms	Complexity [1]	12 sensors [2]	24 sensors [3]
SS-MUSIC	$K^2T + 2(l_V+1)^3 + (l_V+1)^2 + J(l_V+1)(l_V+1-Q)$	2.5×10^6	1.8×10^8
Our algorithm	$K^2T + K^2 - f_V + (l_V+1)^3 + (l_V+1)^2(l_V+1-Q) + (2l_V)^3$	1.0×10^6	5.3×10^7

[1] J is set to obtain 20 angle gird points in a half power beam width of an array, and $f_V = 2l_V + 1$.
[2] $N = 3$, $M = 4$, $l_V = 45$ and $J = 1588$ for the NMRA with 12 physical sensors.
[3] $N = 4$, $M = 6$, $l_V = 157$ and $J = 6176$ for the NMRA with 24 physical sensors.

the data of the repeated virtual elements, and it just needs one multiplication to compute the average value. Because the number of repeated elements in the virtual array is $K^2 - f_V$, the maximum number of multiplications is $K^2 - f_V$ to obtain $\mathbf{z}$ from $\widetilde{\mathbf{z}}$. For SS-MUSIC algorithm, the repeated elements are removed, and hence no multiplication is needed. However the signal power of these repeated elements is lost, and the SNR of the observation data will be decreased simultaneously for SS-MUSIC algorithm.

3) *Decorrelation of the equivalent sources.* The Toeplitz matrix $\mathbf{Y}$ in (30) is used to decorrelate the equivalent sources in our algorithm, and it is just the reorganization of $\mathbf{z}$. Therefore no multiplication is required. However, the computational complexity of $\mathbf{R}_{\mathrm{SS}}$ in (29) is $\mathcal{O}\left((l_V+1)^3 + (l_V+1)^2\right)$, which is much larger than the cost of constructing $\mathbf{Y}$.

4) *Perform EVD on* $\mathbf{Y}$ (30) *or* $\mathbf{R}_{\mathrm{SS}}$ (29) *to obtain the noise subspace and signal subspace.* Since the dimension of $\mathbf{R}_{\mathrm{SS}}$ is the same as the dimension of $\mathbf{Y}$, the computational complexities of EVD on $\mathbf{Y}$ and $\mathbf{R}_{\mathrm{SS}}$ are the same, which is $\mathcal{O}\left((l_V+1)^3\right)$.

5) *DOA estimation.* The roots of a root-MUSIC polynomial is used to estimate the DOAs of the sources in our algorithm. The main computational costs focus on the coefficients and roots computations of the polynomial $f_{\mathrm{MUSIC}}(r)$ (32), and they are $\mathcal{O}\left((l_V+1)^2(l_V+1-Q)\right)$ and $\mathcal{O}\left(2(l_V)^3\right)$ [28], respectively. The computational cost can be much lower when using some real-valued polynomial [29] or Multi-taper root MUSIC method [28]. For the spectral MUSIC algorithm [1], the computational complexity is $\mathcal{O}\left(J(l_V+1)(l_V+1-Q)\right)$, where J is the number of angle girds. J will be very large for a large angle scope and/or a fine angle grid.

The computational complexities of the proposed algorithm and SS-MUSIC are summarized in Table 5. Two examples of 12 and 24 physical sensors are also included, where J is set to obtain 20 angle gird points in a half power beam width of an array. It can be concluded from Table 5 that the computational complexity of our algorithm has been reduced significantly, i.e., it is around 1/3 of that using the SS-MUSIC algorithm for the two examples.

VII. NUMERICAL EXAMPLES

In this section we conduct simulation experiments to evaluate the DOA estimation performance of the GNSA using our proposed DOA algorithm and the SS-MUSIC algorithm described in Section VI.

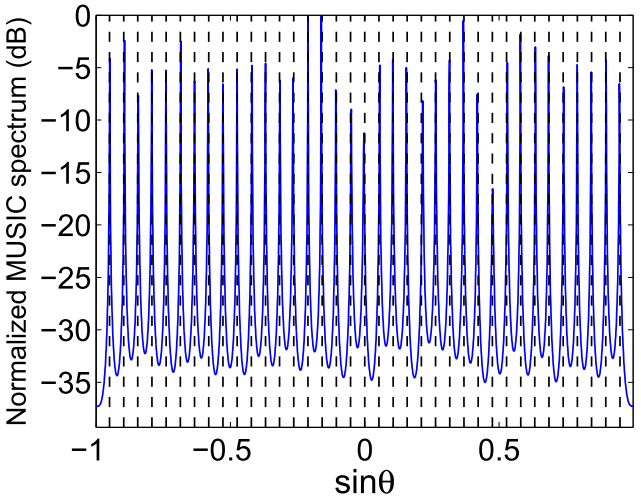

FIGURE 7. MUSIC spectrum as a function of sine of the DOA (Sources number $Q = 37$), using the NMRA with 12 physical sensors. The vertical dash lines are the true positions of the sources.

A. MUSIC SPECTRUM

First we show the ability of the proposed array to resolve more sources than sensors using the SS-MUSIC algorithm. We use the NMRA with 12 physical sensors illustrated in Fig. 2 as an example, and the number of DOF in its DCA is 91. Since the spatial smoothing operation halves the number of DOF in the DCA [10], the available DOF for SS-MUSIC becomes 46. We consider $Q = 37$ uncorrelated, equal power, narrowband sources impinging on the array at spatial frequencies $\sin\theta$, uniformly distributed between -0.95 and 0.95. The number of sources Q is assumed to be known to the system. The spatial MUSIC spectrum of the NMRA is shown in Fig. 7, where 1000 noise-free snapshots are used. The figure shows that the NMRA can resolve all the 37 sources correctly, which is much larger than the number of physical sensors (=12).

B. DOA ESTIMATION ALGORITHMS COMPARISON

In order to compare the estimation performance of our algorithm with the SS-MUSIC algorithm, we use Monte Carlo simulations to evaluate the average root-mean-square error (RMSE) of the estimated DOAs as a function of SNR. The RMSE is defined RMSE $= \sqrt{\frac{1}{Q}\sum_{q=1}^{Q} E(\hat{\theta}_q - \theta_q)^2}$, where $\hat{\theta}_q$ is the estimated value of θ_q. All the following RMSEs are averaged over 500 independent Monte Carlo trials. We use the NMRA in Fig. 2 and consider $Q = 16$ narrowband uncor-

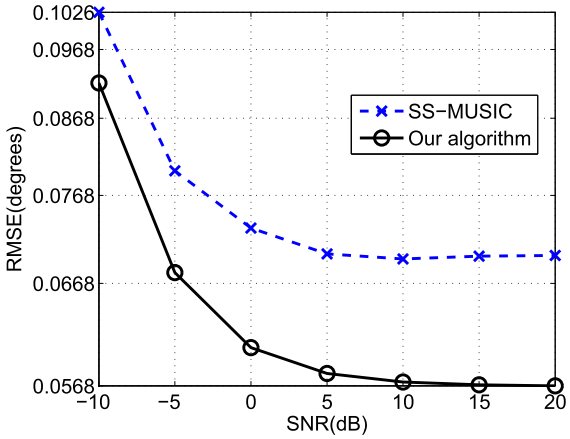

FIGURE 8. DOA estimation performances versus SNR with 12-element NMRA for two algorithms: SS-MUSIC and our proposed algorithm. The number of sources $Q = 16$.

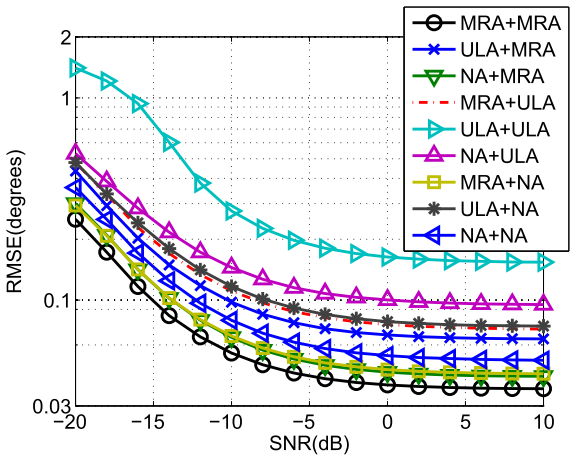

FIGURE 9. DOA estimation performances versus SNR of various GNSA array configurations with 16 physical sensors. The number of sources $Q = 19$.

related sources uniformly distributed between $-45°$ and $45°$. And the angle grid search interval of SS-MUSIC is $0.01°$. Fig. 8 plots the RMSEs of the two algorithms as a function of SNR with 1000 snapshots. It can be seen that our proposed algorithm outperforms the SS-MUSIC algorithm.

The performance improvement of our DOA estimation algorithm mainly depends on the following two aspects. One is that we obtain the observation data of the difference co-arrays by exploiting the data of all virtual elements using a dimension reduction matrix. But the repeated elements are removed in the conventional SS-MUSIC algorithm [7], [9], which may lead to a reduction of SNR. The other is that we adopt a Root-MUSIC algorithm to estimate the DOA instead of the conventional spectral search MUSIC algorithm. It has been shown [26] that the Root-MUSIC algorithm has a better DOA estimation performance than the conventional MUSIC [1] algorithm. Therefore, our proposed algorithm can reach a better DOA estimation performance with a lower computational cost.

When the SNR is low or the number of snapshots is small, the DOA estimation performance of the Root-MUSIC degrades. We can adopt some approach such as pseudo-noise resampling [27], [30] to improve the estimation performance.

C. DOA ESTIMATION PERFORMANCE FOR DIFFERENT ARRAY GEOMETRIES

There are many possible array geometries for the GNSA with a fixed number of physical sensors, *e.g.*, the 16-element geometries illustrated in Fig. 3. Their aperture lengths, the numbers of DOF are various, and hence their DOA estimation performance will also be different. First, we use the GNSA array configurations with 16 physical sensors in Fig. 3 as an example, and compare their DOA estimation performances versus SNR using our proposed DOA estimation algorithm. The simulation results are shown in Fig. 9, where $Q = 19$ narrowband uncorrelated sources uniformly distributed between $-45°$ and $45°$, and the number of snapshots is 500. Fig. 9 shows that the "MRA + MRA" structure obtains the lowest RMSE while the "ULA + ULA" structure has the highest RMSE, and the performances of other arrays are between the former two array structures. By comparing Fig. 9 and Fig. 3, it can be concluded that the RMSEs of DOA estimation for different array geometries are inverse proportional to their aperture lengths.

In addition, the NMRA has been shown to have a larger aperture and a larger number of DOF than the nested array (NA) and the coprime array with compressed inter-element spacing (CACIS) with the same number of physical sensors in Section V. Therefore the NMRA is expected to obtain a better DOA estimation performance. In this example, we use the three array geometries (NA, CACIS, and NMRA) with 24 physical sensors, whose configuration parameters are listed in Table 4, and compare their DOA estimation performances using our proposed DOA estimation algorithm in Section VI. We consider $Q = 16$ narrowband uncorrelated sources uniformly distributed between $-45°$ and $45°$. Fig. 10(a) plots the RMSEs of three array geometries as a function of SNR when the number of snapshots is fixed at 1000, and Fig. 10(b) shows the corresponding performance versus the number of snapshots for SNR $= 0$ dB. The result of the 24-element MRA is not shown owing to the fact that no such array configuration has been published in existing [12]. It can be concluded that the DOA estimation performances improve with the increase of SNR and the number of snapshots. The CACIS has the highest RMSE because it has the shortest aperture, least number of DOF and its DCA is not a hole-free ULA. Our proposed NMRA achieves the best performance with the lowest RMSE in both figures, which shows the superiority of the NMRA in DOA estimation over other array geometries.

D. RESOLUTION PERFORMANCE

The MUSIC algorithm is able to resolve closely spaced sources due to its super-resolution characteristics. Since the

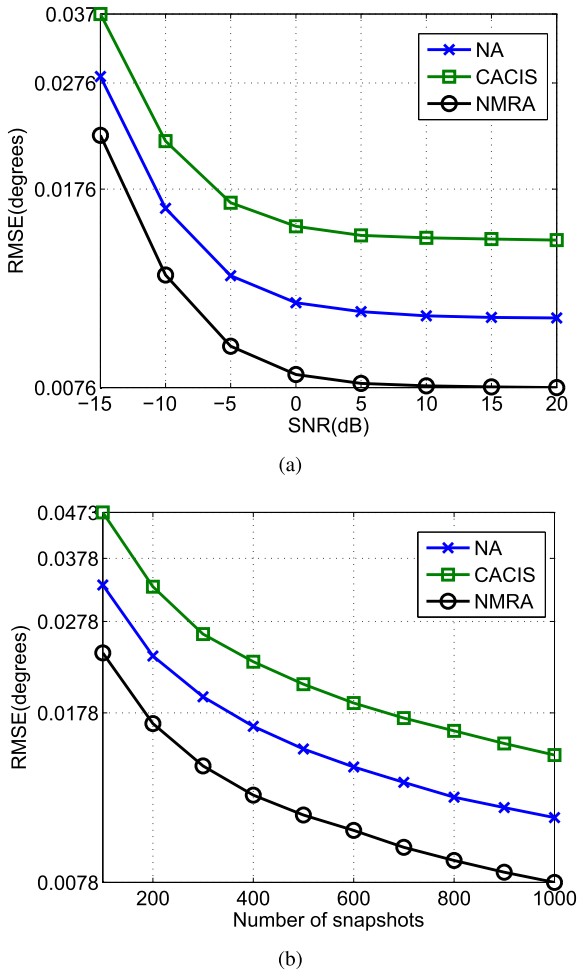

FIGURE 10. DOA estimation performances of different arrays with 24 physical sensors. The number of sources $Q = 16$. (a) RMSE versus SNR (1000 snapshots). (b) RMSE versus number of snapshots (SNR = 0 dB).

proposed NMRA has a larger aperture than the NA and the CACIS, the NMRA is expected to achieve a higher resolution. We use the same three arrays of 24 physical sensors as in Section VII-C, and the apertures of the NA, the CACIS and the NMRA are $155d$, $143d$ and $175d$, respectively. We consider two uncorrelated sources with equal power and angle separation $\Delta\theta = \theta_1 - \theta_2$, where θ_1, θ_2 are the DOAs of two sources. We use the following equation [31] as the resolution analysis criteria

$$\gamma(\theta_1, \theta_2) \triangleq \frac{1}{2}\left[P(\theta_1) + P(\theta_2)\right] - P(\theta_m) > 0, \qquad (34)$$

where $\theta_m = (\theta_1 + \theta_2)/2$ stands for the mid-angle between two sources, and $P(\theta_i)$, $i = 1, 2, \cdots, m$ denotes the MUSIC spectrum at the angle θ_i. We would say that the two signals are resolvable if the inequality (34) holds, and they are irresolvable otherwise. We define the probability of resolution as the probability of $\gamma(\theta_1, \theta_2) > 0$, that is

$$P_{res} = Pr\{\gamma(\theta_1, \theta_2) > 0\}. \qquad (35)$$

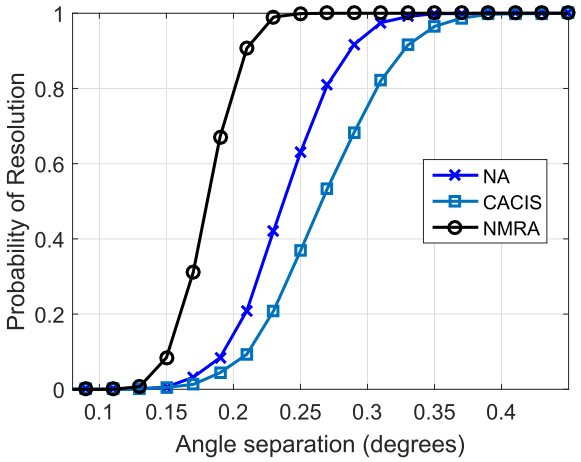

FIGURE 11. Probability of resolution as a function of angle separation for different arrays with 24 physical sensors. The result is obtained over 1000 trials with 100 snapshots and SNR = 0 dB.

Fig. 11 illustrates the variation of the probability of resolution with the angle separation $\Delta\theta$, which is obtained over 1000 Monte Carlo runs with 100 snapshots at SNR = 0dB. It can be seen that the probabilities of resolution for the three array geometries improve with the increase of the angle separation, and all of them can reach 100% when the angle separation is larger than 0.4°. Our proposed NMRA outperforms the NA and the CACIS when the angle separation between 0.13° and 0.35°. We define the *resolution threshold* of an array as the minimum angle separation at which the probability of resolution reaches one. In Fig. 11, the resolution threshold of the NMRA is 0.25°, which is lower than the resolution threshold of the NA and the CACIS. This demonstrates that the NMRA has better resolution performance due to its larger aperture.

VIII. CONCLUSION

In this paper we proposed a unified array geometry, dubbed generalized nested subarray (GNSA), which can be easily constructed by the cross summation of two subarrays. It is possible to predict the sensor positions and the number of DOF when these parameters of the subarrays are given. We have derived the aperture length of a GNSA, the number of DOF in its DCA, and have unveiled the parameter relationship of a GNSA with its subarray configurations. We have used the nested MRA (NMRA) as an example to compare its characteristics with the nested array and the coprime array. The simulation results have demonstrated that the NMRA has a larger aperture as well as a higher number of DOF than the two-level nested array and the CACIS with the same number of physical sensors. Furthermore, the NMRA enjoys lower mutual coupling than the nested array.

In order to overcome the limitations of the existing underdetermined DOA estimation algorithms, we develop a new DOA estimation algorithm for the GNSA. The new algorithm has achieved better DOA estimation performance than

traditional SS-MUSIC algorithm with lower computational cost. We demonstrate the superiorities of the proposed array in resolving more sources than sensors, DOA estimation performance, and probability of resolution using the new algorithm over the SS-MUSIC algorithm.

One shortcoming of the proposed array geometry is that the new array relies on the structures of the known subarrays, and therefore not all GNSA geometries with any number of sensors can be obtained. For example, when the total number of sensors is a prime number, it is impossible to construct a GNSA. However, the new array geometry provides a closed-form solution to generate a suboptimal coarray, and can easily provide a larger array employing the known MRA. In addition, owing to the structure of multiple identical subarray, the GNSA enjoys some advantages in real applications, such as low cost and easy extension to a larger array, *etc*.

APPENDIX A
PROOF OF PROPOSITION 1

The location set $\mathbb{V}_V$ of the virtual array generated from a GNSA can be calculated by (8). Substituting (11) into (8), we obtain

$$\begin{aligned}\mathbb{V}_V &= \{\left(n_j \cdot D + m_i \cdot d\right) - \left(n_{j'} \cdot D + m_{i'} \cdot d\right), \\ &\qquad 1 \le j, j' \le N,\ 1 \le i, i' \le M\} \\ &= \left\{(n_j - n_{j'})D + (m_i - m_{i'})d\right\} \\ &= \mathbb{V}_B \oplus \mathbb{V}_A. \end{aligned} \tag{36}$$

where $\mathbb{V}_B = \{(n_j - n_{j'})D,\ 1 \le j, j' \le N\}$ and $\mathbb{V}_A = \{(m_i - m_{i'})d,\ 1 \le i, i' \le M\}$ are the location set forming the virtual array of `Subarray B` and `Subarray A`, respectively. Thus, the location set of the virtual array generated from a GNSA can be calculated by the cross summation of $\mathbb{V}_B$ and $\mathbb{V}_A$.

We have defined in Section II that the location set $\mathbb{D}$ of the DCA of a linear array only contains the unique elements of the location set $\mathbb{V}$ of its virtual array. We denote the location sets of the DCA associated with the GNSA, `Subarray B` and `Subarray A` as $\mathbb{D}_V$, $\mathbb{D}_B$ and $\mathbb{D}_A$, respectively. The DCAs of both `Subarray B` and `Subarray A` are hole-free ULAs with symmetric property in our definition. Therefore, $\mathbb{D}_B$ and $\mathbb{D}_A$ can be expressed respectively as

$$\begin{aligned}\mathbb{D}_B &= \{nD = nLd, -l_B \le n \le l_B\}, \\ \mathbb{D}_A &= \{md, -l_A \le m \le l_A\}. \end{aligned} \tag{37}$$

where $D = Ld$, L is an integer, l_B and l_A are the aperture length of Subarrays B and A, respectively.

Combining (36) and (37), we obtain

$$\begin{aligned}\mathbb{D}_V &= \{(nL + m)d, -l_B \le n \le l_B, -l_A \le m \le l_A\} \\ &= \mathbb{D}_B \oplus \mathbb{D}_A. \end{aligned} \tag{38}$$

Therefore, $\mathbb{D}_V$ can also be calculated by the cross summation of $\mathbb{D}_B$ and $\mathbb{D}_A$.

APPENDIX B
PROOF OF PROPOSITION 2

The number of DOF is equal to the number of distinct elements in the location set. From (37) we can obtain the relations between the number of DOF and the aperture length of `Subarray B` and `Subarray A` respectively, that is $f_A = 2l_A + 1, f_B = 2l_B + 1$. Next, we prove Proposition 2 using the following three steps.

1) There are $2l_A + 1\ (= f_A)$ possible consecutive integers for m in (38). Thus the item $nL + m$ are consecutive integers when $L = f_A$, which leads to the fact that the DCA of the GNSA is a hole-free ULA if $D = f_A \cdot d$. However if $L > f_A$, there will be some missed integers for the item $nL + m$, that is there will be holes in the DCA. Hence the DCA is not a hole-free ULA. On the contrary, $L < f_A$ will result in additional overlapped elements. Therefore when $L = f_A$, the DCA of the GNSA is a hole-free ULA with minimum overlapped elements (that is minimum redundancies).
   For example, if $L = f_A + 1$, then there will be holes appeared at locations $(n+1)l_A + l_A + 1$ between $nL + l_A$ and $(n+1)L - l_A$ for $-l_B \le n \le l_B - 1$. If letting $L = f_A - 1$, we can obtain $nL + l_A = (n+1)L - l_A$ for $-l_B \le n \le l_B - 1$ by substituting $f_A = 2l_A + 1$. Thus there are additional $f_B - 1$ redundancies than the case of $L = f_A$.
2) From (11) we know that the aperture length of a GNSA is $l_B \cdot D + l_A \cdot d$. Substituting $D = f_A \cdot d$, we get
$$l_V \cdot d = (l_B \cdot f_A + l_A)\, d. \tag{39}$$
3) The DCA of a GNSA is a hole-free ULA with elements located within the range of $[-l_V, l_V]\, d$. Therefore the aperture length of the DCA is $(2l_V + 1)d = f_V \cdot d$, and the number of DOF in the DCA is
$$\begin{aligned} f_V &= 2l_V + 1 = 2f_A \cdot l_B + 2l_A + 1 \\ &= 2f_A \cdot l_B + f_A = f_A \cdot (2l_B + 1) \\ &= f_A \cdot f_B. \end{aligned} \tag{40}$$

APPENDIX C
PROOF OF WEIGHT FUNCTION

By (36) and (38) we know that the number of times that $k = (nL + m)d$ occurs in $\mathbb{V}_V$ depends on the number of times that n occurs in $\mathbb{V}_B$ and m occurs in $\mathbb{V}_A$, which are the weight function $\mathbf{w}_B(n)$ and $\mathbf{w}_A(m)$, respectively. For example, if n occurs two times in $\mathbb{V}_B$ and only one m appears in $\mathbb{V}_A$, then the $k = (nL + m)d$ will occur two times in $\mathbb{V}_V$. Thus,

$$\begin{aligned}\mathbf{w}_V(nL + m) = \mathbf{w}_B(n) \cdot \mathbf{w}_A(m), \\ -l_B \le n \le l_B,\ -l_A \le m \le l_A. \end{aligned} \tag{41}$$

Traversing all n and m, we can obtain the weight function $\mathbf{w}_V$ of the GNSA

$$\mathbf{w}_V = \mathbf{w}_B \otimes \mathbf{w}_A, \tag{42}$$

where $\otimes$ stands for the Kronecker product.

APPENDIX D
PROOF OF (26)

The matrix $\mathbf{E}$ is a column orthogonal matrix owing to that every row of $\mathbf{E}$ is a unitary vector. The (i, j)-th element of $\mathbf{E}^T\mathbf{E}$ is the product of i-th column and j-th column. Thus the non-diagonal elements of $\mathbf{E}^T\mathbf{E}$, where $i \neq j$, are zeros. Therefore $\mathbf{E}^T\mathbf{E}$ is a diagonal matrix.

Every diagonal element of $\mathbf{E}^T\mathbf{E}$ is the quadratic summation of elements in the corresponding column of $\mathbf{E}$. Since the elements of $\mathbf{E}$ are 0 or 1, the quadratic summation of elements in $\mathbf{E}$ is equal to the summation of the corresponding elements. Thus the diagonal elements of $\mathbf{E}^T\mathbf{E}$ are the summation of elements in the corresponding column of $\mathbf{E}$, which are equal to the value of weight function $\mathbf{w}$ defined in Section III.

APPENDIX E
PROOF FOR THEOREM 1

$\mathbf{z}$ is the equivalent received data of a hole-free ULA with elements located at the range of $[-l_V, l_V]\,d$. Omitting the noise, the i-th element of $\mathbf{z}$ can be expressed by

$$z_i = \sum_{q=1}^{Q} e^{j\kappa(i-l_V-1)\sin\theta_q} \cdot \sigma_q^2 = \mathbf{g}_{Qi}^T \mathbf{D}^{-l_V-1}\mathbf{c}, \tag{43}$$

where $\mathbf{g}_{Qi} = \left[e^{j\kappa i \sin\theta_1}, e^{j\kappa i \sin\theta_2}, \cdots, e^{j\kappa i \sin\theta_Q}\right]^T$, $\mathbf{D} = \text{Diag}\left[e^{j\kappa \sin\theta_1}, e^{j\kappa \sin\theta_2}, \cdots, e^{j\kappa \sin\theta_Q}\right]$. The following relations hold for $\mathbf{g}_{Qi}$ and $\mathbf{D}$

$$\begin{aligned}
&\mathbf{g}_{Q0} = [1, 1, \cdots, 1]^T \in \mathbb{C}^{Q\times 1},\\
&\mathbf{g}_{Q1} = \text{diag}\,(\mathbf{D}),\\
&\mathbf{g}_{Qi} = \mathbf{g}_{Q(i-1)}\mathbf{D} = \text{diag}\left(\mathbf{D}^i\right),\\
&\qquad\qquad i = 1, 2, \cdots, 2l_V + 1.
\end{aligned} \tag{44}$$

The first column of $\mathbf{Y}$ is

$$\begin{aligned}
\mathbf{y}_{c1} &= \left[z_{l_V+1}, z_{l_V+2}, \cdots, z_{2l_V+1}\right]^T\\
&= \left[\mathbf{g}_{Q0}, \mathbf{g}_{Q1}, \cdots, \mathbf{g}_{Ql_V}\right]^T \mathbf{c}\\
&= \mathbf{G}_1\mathbf{c},
\end{aligned} \tag{45}$$

where $\mathbf{G}_1 = \left[\mathbf{g}_{Q0}, \mathbf{g}_{Q1}, \cdots, \mathbf{g}_{Ql_V}\right]^T \in \mathbb{C}^{(l_V+1)\times Q}$. We observe that $\mathbf{G}_1$ is a $(l_V + 1) \times Q$ Vandermonde matrix. Therefore the rank of $\mathbf{G}_1$ is Q (we have assumed that $l_V + 1 > Q$).

Then i-th column of $\mathbf{Y}$ is

$$\begin{aligned}
\mathbf{y}_{ci} &= \left[z_{l_V-i+2}, z_{l_V-i+3}, \cdots, z_{2l_V-i+2}\right]^T\\
&= \mathbf{G}_1\mathbf{D}^{-i+1}\mathbf{c}.
\end{aligned} \tag{46}$$

Therefore,

$$\begin{aligned}
\mathbf{Y} &= \left[\mathbf{y}_{c1}, \mathbf{y}_{c2}, \cdots, \mathbf{y}_{c(l_V+1)}\right]\\
&= \left[\mathbf{G}_1\mathbf{c}, \mathbf{G}_1\mathbf{D}^{-1}\mathbf{c}, \cdots, \mathbf{G}_1\mathbf{D}^{-l_V}\mathbf{c}\right]\\
&= \mathbf{G}_1\mathbf{C}\left[\mathbf{g}_{Q0}^*, \mathbf{g}_{Q1}^*, \cdots, \mathbf{g}_{Ql_V}^*\right]\\
&= \mathbf{G}_1\mathbf{C}\mathbf{G}_1^H,
\end{aligned} \tag{47}$$

where $\mathbf{C} = Diag(\mathbf{c}) \in \mathbb{C}^{Q\times Q}$ is a diagonal matrix of signal powers. Because the signal powers of sources are not zeros, the rank of $\mathbf{C}$ is Q.

From the above analysis, we know that the ranks of $\mathbf{G}_1$ and $\mathbf{C}$ are both equal to Q.

From (28) we know that noise only exists at the $(l_V + 1)$-th element of $\mathbf{z}$, *i.e.*, z_{l_V+1}. Therefore when considering noise, $\mathbf{Y}$ can be expressed as

$$\mathbf{Y} = \mathbf{G}_1\mathbf{C}\mathbf{G}_1^H + \sigma_n^2\mathbf{I}, \tag{48}$$

where $\mathbf{I}$ is a $(l_V + 1) \times (l_V + 1)$ identity matrix. Because the identity matrix $\mathbf{I}$ is a full rank matrix, and its eigenvectors can be any vectors with size $(l_V + 1) \times 1$. The item $\sigma_n^2\mathbf{I}$ will enhance the rank of $\mathbf{Y}$ to $l_V + 1$. Thus, $\mathbf{Y}$ is a full rank matrix independent of the coherency of the sources. And the eigenvectors corresponding to the first Q-largest eigenvalues form the signal subspace.

REFERENCES

[1] R. O. Schmidt, "Multiple emitter location and signal parameter estimation," *IEEE Trans. Antennas Propag.*, vol. AP-34, no. 3, pp. 276–280, Mar. 1986.

[2] R. Roy and T. Kailath, "Esprit-estimation of signal parameters via rotational invariance techniques," *IEEE Trans. Acoust., Speech, Signal Process.*, vol. 37, no. 7, pp. 984–995, Jul. 1989.

[3] Z.-Q. He, Z.-P. Shi, H. C. So, and L. Huang, "Underdetermined DOA estimation for wideband signals using robust sparse covariance fitting," *IEEE Signal Process. Lett.*, vol. 22, no. 4, pp. 435–439, Apr. 2015.

[4] W.-K. Ma, T.-H. Hsieh, and C.-Y. Chi, "DOA estimation of quasi-stationary signals with less sensors than sources and unknown spatial noise covariance: A Khatri–Rao subspace approach," *IEEE Trans. Signal Process.*, vol. 58, no. 4, pp. 2168–2180, Apr. 2010.

[5] K. Xiong, Z. Liu, Z. Liu, D. Feng, and W. Jiang, "Underdetermined DOA estimation of multi-path signals based on ICA and sparse reconstruction," in *Proc. IEEE Int. Conf. Acoust., Speech Signal Process. (ICASSP)*, May 2014, pp. 2233–2236.

[6] Z. Tan, Y. C. Eldar, and A. Nehorai, "Direction of arrival estimation using co-prime arrays: A super resolution viewpoint," *IEEE Trans. Signal Process.*, vol. 62, no. 21, pp. 5565–5576, Nov. 2014.

[7] P. Pal and P. P. Vaidyanathan, "Nested arrays: A novel approach to array processing with enhanced degrees of freedom," *IEEE Trans. Signal Process.*, vol. 58, no. 8, pp. 4167–4181, Aug. 2010.

[8] A. Moffet, "Minimum-redundancy linear arrays," *IEEE Trans. Antennas Propag.*, vol. AP-16, no. 2, pp. 172–175, Mar. 1968.

[9] P. P. Vaidyanathan and P. Pal, "Sparse sensing with co-prime samplers and arrays," *IEEE Trans. Signal Process.*, vol. 59, no. 2, pp. 573–586, Feb. 2011.

[10] S. Qin, Y. D. Zhang, and M. G. Amin, "Generalized coprime array configurations for direction-of-arrival estimation," *IEEE Trans. Signal Process.*, vol. 63, no. 6, pp. 1377–1390, Mar. 2015.

[11] M. Yang, A. M. Haimovich, B. Chen, and X. Yuan, "A new array geometry for DOA estimation with enhanced degrees of freedom," in *Proc. IEEE Int. Conf. Acoust., Speech Signal Process. (ICASSP)*, Mar. 2016, pp. 3041–3045.

[12] H. L. Van Trees, *Optimum Array Processing: Part IV of Detection, Estimation, and Modulation Theory*. New York, NY, USA: Wiley, 2002.

[13] M. Ishiguro, "Minimum redundancy linear arrays for a large number of antennas," *Radio Sci.*, vol. 15, no. 6, pp. 1163–1170, 1980.

[14] P. Pal and P. P. Vaidyanathan, "Multiple level nested array: An efficient geometry for 2qth order cumulant based array processing," *IEEE Trans. Signal Process.*, vol. 60, no. 3, pp. 1253–1269, Mar. 2012.

[15] E. BouDaher, Y. Jia, F. Ahmad, and M. G. Amin, "Multi-frequency co-prime arrays for high-resolution direction-of-arrival estimation," *IEEE Trans. Signal Process.*, vol. 63, no. 14, pp. 3797–3808, Jul. 2015.

[16] P. Pal and P. P. Vaidyanathan, "Coprime sampling and the MUSIC algorithm," in *Proc. IEEE Digital Signal Process. Workshop, IEEE Signal Process. Edu. Workshop (DSP/SPE)*, Jan. 2011, pp. 289–294.

[17] Z. Tan and A. Nehorai, "Sparse direction of arrival estimation using co-prime arrays with off-grid targets," *IEEE Signal Process. Lett.*, vol. 21, no. 1, pp. 26–29, Jan. 2014.
[18] Y. D. Zhang, M. G. Amin, and B. Himed, "Sparsity-based DOA estimation using co-prime arrays," in *Proc. IEEE Int. Conf. Acoust., Speech Signal Process. (ICASSP)*, May 2013, pp. 3967–3971.
[19] E. BouDaher, F. Ahmad, and M. G. Amin, "Sparsity-based direction finding of coherent and uncorrelated targets using active nonuniform arrays," *IEEE Signal Process. Lett.*, vol. 22, no. 10, pp. 1628–1632, Oct. 2015.
[20] C.-L. Liu and P. P. Vaidyanathan, "Super nested arrays: Sparse arrays with less mutual coupling than nested arrays," in *Proc. IEEE Int. Conf. Acoust., Speech Signal Process. (ICASSP)*, Mar. 2016, pp. 2976–2980.
[21] V. I. Vasylyshyn and O. A. Garkusha, "Direction finding using sparse array composed of multiple identical subarrays," in *Proc. 5th Int. Conf. Antenna Theory Techn.*, May 2005, pp. 273–276.
[22] K. T. Wong and M. D. Zoltowski, "Direction-finding with sparse rectangular dual-size spatial invariance array," *IEEE Trans. Aerosp. Electron. Syst.*, vol. 34, no. 4, pp. 1320–1336, Oct. 1998.
[23] K. T. Wong and M. D. Zoltowski, "Sparse array aperture extension with dual-size spatial invariances for ESPRIT-based direction finding," in *Proc. IEEE 39th Midwest Symp. Circuits Syst.*, vol. 2. Aug. 1996, pp. 691–694.
[24] S. U. Pillai and B. H. Kwon, "Forward/backward spatial smoothing techniques for coherent signal identification," *IEEE Trans. Acoust., Speech Signal Process.*, vol. 37, no. 1, pp. 8–15, Jan. 1989.
[25] C. L. Liu and P. P. Vaidyanathan, "Remarks on the spatial smoothing step in coarray MUSIC," *IEEE Signal Process. Lett.*, vol. 22, no. 9, pp. 1438–1442, Sep. 2015.
[26] B. D. Rao and K. V. S. Hari, "Performance analysis of root-music," *IEEE Trans. Acoust., Speech, Signal Process.*, vol. 37, no. 12, pp. 1939–1949, Dec. 1989.
[27] C. Qian *et al.*, "Improved unitary root-MUSIC for DOA estimation based on pseudo-noise resampling," *IEEE Signal Process. Lett.*, vol. 21, no. 2, pp. 140–144, Feb. 2014.
[28] J. Wu, T. Wang, and Z. Bao, "Fast realization of root MUSIC using multi-taper real polynomial rooting," *Signal Process.*, vol. 106, pp. 55–61, Jan. 2015.
[29] J. Selva, "Computation of spectral and root MUSIC through real polynomial rooting," *IEEE Trans. Signal Process.*, vol. 53, no. 5, pp. 1923–1927, May 2005.
[30] V. Vasylyshyn, "Removing the outliers in root-MUSIC via pseudo-noise resampling and conventional beamformer," *Signal Process.*, vol. 93, no. 12, pp. 3423–3429, 2013.
[31] Q. T. Zhang, "Probability of resolution of the MUSIC algorithm," *IEEE Trans. Signal Process.*, vol. 43, no. 4, pp. 978–987, Apr. 1995.

MINGLEI YANG (M'14) received the B.E. degree in electronic engineering and the Ph.D. degree in signal and information processing from Xidian University in 2004 and 2009, respectively. Since 2009, he has been with the National Laboratory of Radar Signal Processing, Xidian University, where he is currently an Associate Professor. From 2014 to 2015, he was a Visiting Scholar with the Elisha Yegal Bar-Ness Center for Wireless Communications and Signal Processing Research, New Jersey Institute of Technology. He has been doing research in the fields of array signal processing, MIMO signal processing, and polarization information processing. He has published over 60 peer-reviewed journals and conference papers, and over 40 inventions.

ALEXANDER M. HAIMOVICH (S'82–M'87–F'13) received the B.Sc. degree in electrical engineering from the Technion–Israel Institute of Technology, Haifa, in 1977, the M.Sc. degree in electrical engineering from Drexel University, Philadelphia, in 1983, and the Ph.D. degree in systems from the University of Pennsylvania, Philadelphia, in 1989. From 1983 to 1990, he was a Design Engineer and a Staff Consultant with AEL Industries. He served as a Chief Scientist of JJM systems from 1990 to 1992. Since 1992, he has been on the Faculty of the New Jersey Institute of Technology, where he currently serves as the Ying Wu Chair and a Distinguished Professor with the Electrical and Computer Engineering Department. He also serves as the Director of the Elisha Bar-Ness Center for Wireless Information Processing. His research interests include MIMO radar, active and passive localization, signal intelligence, sensor networks, and wireless networks.

XIN YUAN (S'09–M'12–SM'16) received the B.Eng. and M.Eng. degrees from Xidian University in 2007 and 2009, respectively, and the Ph.D. degree from The Hong Kong Polytechnic University in 2012. From 2012 to 2015, he was a Post-Doctoral Associate with the Department of Electrical and Computer Engineering, Duke University. Since 2015, he has been a Video Analysis and Coding Lead Researcher with Bell Labs, Murray Hill, NJ, USA. He is the author of two book chapters, over 70 articles, and over 10 inventions. His research interests include signal processing, computational photography, image processing, machine learning, and computer vision. He develops compressive sensing techniques for high-dimensional imaging with applications to videos, hyperspectral, microscopy, and x-ray imaging systems. Two papers he co-authored received the Best Paper Award from the Computational Optical Sensing and Imaging Conferences in 2013 and 2014, on video compressive sensing and on depth compressive sensing cameras, respectively.

LEI SUN received the B.E. degree in electronic information engineering from the Jiangsu University of Science and Technology in 2015. He is currently pursuing the master's degree with the National Laboratory of Radar Signal Processing, Xidian University. His research interests include radar signal processing and array signal processing.

BAIXIAO CHEN was born in Anhui, China, in 1966. He received the degree from the Metallurgy College of East China in 1987, and the master's degree in circuit and system and the Ph.D. degree in signal and information processing from Xidian University, in 1994 and 1997, respectively. From 1987 to 1991, he was with the Metallurgy College of East China. Since 1997, he has been a Faculty Member with the National Laboratory of Radar Signal Processing, Xidian University. He was a Lecturer and an Associate Professor from 1997 to 1999 and from 1996 to 2003, respectively. In 2006, he was selected into the New Century elitist Support Program of the ministry of education. He is currently a Professor on signal and information processing. His general research interests include radar signal processing, new radar system design, array signal processing, precise guidance, and so on.